

BNL 50435
(ENDF-207)

NEUTRON AND GAMMA-RAY PRODUCTION CROSS-SECTIONS FOR NICKEL

M.R. BHAT

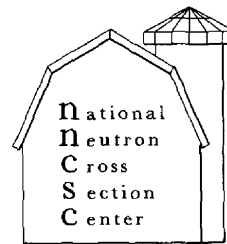
October 1974

BROOKHAVEN
NATIONAL LABORATORY
RESEARCH LIBRARY

04

MAR 19 1975

NATIONAL NEUTRON CROSS SECTION CENTER
BROOKHAVEN NATIONAL LABORATORY
UPTON, NEW YORK 11973



The Energy Research and Development Administration (ERDA) is the successor to the U.S. Atomic Energy Commission (AEC) and all references to the AEC herein shall be deemed to refer to ERDA.



NOTICE

This report was prepared as an account of work sponsored by the United States Government. Neither the United States nor the United States Atomic Energy Commission, nor any of their employees, nor any of their contractors, subcontractors, or their employees, makes any warranty, express or implied, or assumes any legal liability or responsibility for the accuracy, completeness or usefulness of any information, apparatus, product or process disclosed, or represents that its use would not infringe privately owned rights.

Printed in the United States of America
Available from
National Technical Information Service
U.S. Department of Commerce
5285 Port Royal Road
Springfield, VA 22161
Price: Printed Copy \$5.45; Microfiche \$1.45

December 1974

525 copies

BNL 50435
(ENDF-207)
(Physics - TID-4500)

**NEUTRON AND GAMMA-RAY PRODUCTION
CROSS-SECTIONS FOR NICKEL**

M.R. BHAT



October 1974

**NATIONAL NEUTRON CROSS SECTION CENTER
BROOKHAVEN NATIONAL LABORATORY
ASSOCIATED UNIVERSITIES, INC.
UNDER CONTRACT NO. AT(30-1)-16 WITH THE
UNITED STATES ATOMIC ENERGY COMMISSION**

Contents	Page
1. Introduction	1
2. General Properties of Nickel Isotopes	3
3. Neutron Cross-Sections	6
4. Angular Distribution of Secondary Neutrons	40
5. Energy Distribution of Secondary Neutrons	45
6. Gamma-Ray Production Cross-Sections	48
Acknowledgement	54
References	55

List of Tables

No.	Title	Page
1.	Properties of the Naturally Occurring Nickel Isotopes.	63
2.	Reaction Q-values for the Nickel Isotopes.	63
3.	The Elastic Scattering Cross-Section for Nickel.	64
4.	The Non-elastic Scattering Cross-Section for Nickel.	66
5.	The Total Inelastic Scattering Cross-Section for Nickel.	67
6.	The Optical Model Parameters.	68
7.	Summary of Data on (n,n'p), (n,pn') and (n,d) Cross- Sections for Nickel.	69
8.	Error Estimates of the Evaluated Cross-Sections of Ni.	70

List of Illustrations

No.	Title	Page
1	Energy Levels of ^{58}Ni	4
2	Energy Levels of ^{60}Ni	4
3	Energy Levels of ^{62}Ni	5
4	Energy Levels of ^{64}Ni	5
5	Nickel Total Cross-Section 0.7 - 1.0 MeV	7
6	Nickel Total Cross-Section 1.0 - 1.5 MeV	8
7	Nickel Total Cross-Section 1.5 - 2.0 MeV	9
8	Nickel Total Cross-Section 2.0 - 3.0 MeV	10
9	Nickel Total Cross-Section 3.0 - 5.0 MeV	11
10	Nickel Total Cross-Section 5.0 - 11.0 MeV	12
11	Nickel Total Cross-Section 11.0 - 20.0 MeV	13
12	Nickel Elastic Cross-Section 0.7 - 1.0 MeV	16
13	Nickel Elastic Cross-Section 1.0 - 1.5 MeV	16
14	Nickel Elastic Cross-Section 1.5 - 2.0 MeV	16
15	Nickel Elastic Cross-Section 2.0 - 3.0 MeV	16
16	Nickel Elastic Cross-Section 3.0 - 5.0 MeV	17
17	Nickel Elastic Cross-Section 5.0 - 20.0 MeV	17
18	Nickel Non-Elastic Cross-Section	17
19	Nickel Total Inelastic Cross-Section	17
20	Nickel Inelastic Cross-Section $E_{\text{ex}} = 1.172$ MeV	21
21	Nickel Inelastic Cross-Section $E_{\text{ex}} = 1.332$ MeV	21
22	Nickel Inelastic Cross-Section $E_{\text{ex}} = 1.454$ MeV	21
23	Capture Cross-Section of Nickel	25
24	^{58}Ni (n,2n) Cross-Section	25

List of Illustrations (con't)

No.	Title	Page
25	Ni (n,2n) Cross Section	29
26	^{60}Ni (n,p) Cross-Section	33
27	^{61}Ni (n,p) Cross-Section	33
28	^{62}Ni (n,p) Cross-Section	33
29	Ni (n,p) Cross-Section	33
30	Ni (n, α) Cross-Section	36
31	Ni (n,n'p) Cross-Section	39
32	Differential Elastic Scattering of Ni $E_n = 4.34 - 8.56$ MeV	43
33	Differential Inelastic Scattering of ^{58}Ni $E_{ex} = 1.454$ MeV	43
34	Differential Inelastic Scattering of ^{60}Ni $E_{ex} = 1.333$ MeV	44
35	Differential Inelastic Scattering of ^{60}Ni $E_{ex} = 1.333$ MeV	44
36	Differential Inelastic Scattering of ^{60}Ni $E_{ex} = 1.333$ MeV	44
37	Differential Inelastic Scattering of Ni $E_n = 14$ MeV	44
38	Energy Distribution of Continuum Scattering $E_n = 14$ MeV	47
39	Normalized Gamma-ray spectrum at Thermal Energies	51
40	Normalized Gamma-ray Spectrum $E_n = 4$ keV	51
41	Gamma-Ray Production Cross-Section $E_n = 1-17$ MeV	51
42	Ni (n, $x\gamma$) Spectrum $E_n = 4.0$ MeV	53
43	Ni (n, $x\gamma$) Spectrum $E_n = 14.0$ MeV	53
44	Ni (n, $x\gamma$) Spectrum $E_n = 17.0$ MeV	53

1. INTRODUCTION

This report describes the evaluation of the neutron cross-section and the gamma-ray production data on nickel. The available data as of mid-1973 have been included in this evaluation. In addition, an attempt has been made to estimate the errors in the various cross-sections in the different energy ranges. These are reproduced in Table 8 at the end of this report.

This is essentially a new evaluation from $1.0 \text{ E} - 05 \text{ eV}$ to 20.0 MeV except for the resolved resonance parameter data which along with the background cross-sections have been taken over from the ENDF/B-III nickel evaluation (MAT No. 1123). These resonance parameters are by Stieglitz et al¹ and were arrived at by a careful analysis of the experimental data on total and capture cross-sections. The resonance parameters are given only for the four even-even isotopes of nickel. Thus, the contribution of ^{61}Ni with a fractional abundance of 0.011 is considered negligible.

The neutron and gamma-ray production cross-sections given in this nickel evaluation (MAT = 1190 of ENDF/B-IV) over the neutron energy range $1.0 \text{ E} - 05 \text{ eV}$ to 20.0 MeV may be summarized as follows:

File 1: General description of the evaluation with references.

File 2: Resolved resonance parameters for $^{58,60,62,64}\text{Ni}$ from $1.0 \text{ E} - 05 \text{ eV}$ to 690 keV .

File 3: Smooth cross-sections for total, elastic, total inelastic, inelastic cross-sections to some fifteen discrete levels, the inelastic continuum, $(n,2n)$, $(n,n'p)$, (n,p) , (n,α) and capture cross-sections. Also are included data on $\bar{\mu}$, ξ and γ generated from the differential angular distributions given in File 4.

- File 4: Angular distribution for elastic scattering expressed as Legendre polynomial coefficients, with the inelastic scattering assumed to be isotropic.
- File 5: Secondary neutron energy distribution for the inelastic continuum, (n,2n) and (n,n'p) reactions.
- File 12: Multiplicities for gamma ray production due to capture from 1.0E - 05 eV to 1.0 MeV.
- File 13: Gamma production cross-section due to all non-elastic processes from 1.0 - 20.0 MeV.
- File 14: Angular distribution for photons which is assumed to be isotropic.
- File 15: Normalized energy distributions of the photon spectra.

2. General Properties of Nickel Isotopes

2.1. Isotopic Masses and Possible Neutron Induced Reactions

Natural nickel is made up of five isotopes: ^{58}Ni , ^{60}Ni , ^{61}Ni , ^{62}Ni and ^{64}Ni . Their fractional abundances² and isotopic masses³ on the ^{12}C scale are given in Table 1. The properties of natural nickel are essentially determined by those of ^{58}Ni and ^{60}Ni - the most abundant of the isotopes; and all the isotopes except ^{61}Ni are even-even. The nuclear masses are from the recent compilation of Wapstra and Gove.³ Using these data it is also possible to calculate the Q-values for the different possible nuclear reactions induced by neutrons up to a maximum energy of 20.0 MeV. These are listed in Table 2. However, the Q-values for the capture reaction in ^{61}Ni , ^{62}Ni and ^{64}Ni are by Fanger et al,⁴ and Cochavi et al.⁵ The $^{64}\text{Ni}(n,\gamma)$ Q-value is in good agreement with that observed by Arnell et al.⁶

Some of these reaction cross-sections are very small in the energy range of interest or there are no data on them. Hence, they have been left out of the evaluated data files. The only (n, particle) cross-sections given in the data files are for (n,2n), (n,n'p), (n,p) and (n, α) reactions.

The properties of the ground state and the excited states of the even-even nickel isotopes are shown in Figs. 1-4. They were obtained from the latest compilation of the Nuclear Data Group⁷ at ORNL. At level energies higher than those shown here, the spin-parity assignments have not been made or are doubtful. Hence, in the nuclear model calculations to be described later, nuclear levels above 3.5 MeV excitation energy are described by a continuum level density distribution instead of being treated as discrete levels.

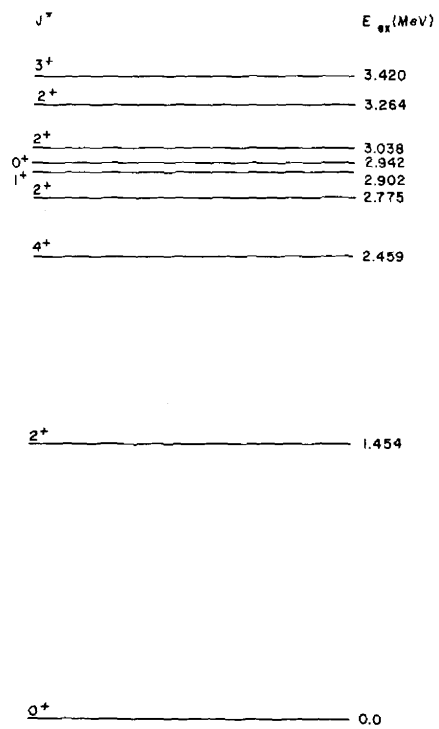


Fig. 1. Energy Levels of ^{58}Ni

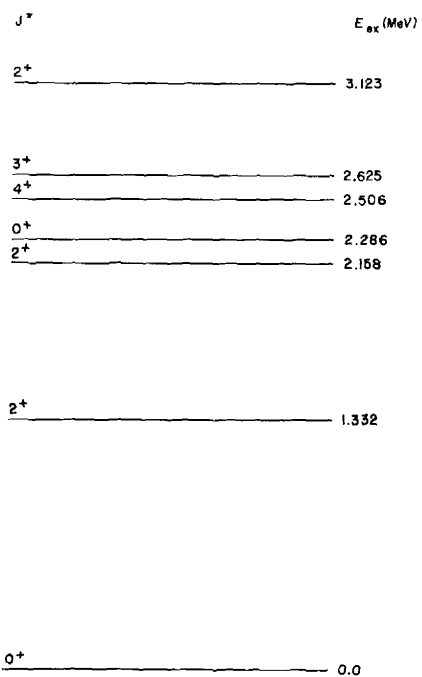


Fig. 2. Energy Levels of ^{60}Ni

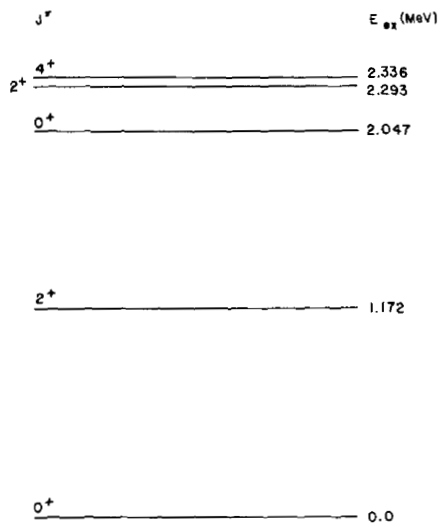


Fig. 3. Energy Levels of ^{62}Ni

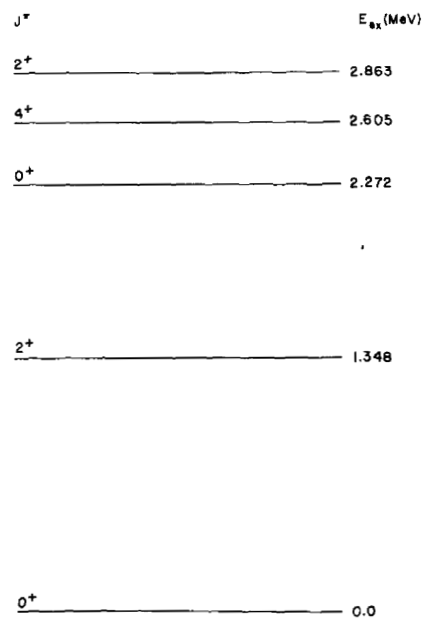


Fig. 4. Energy Levels of ^{64}Ni

3. Neutron Cross-Sections

3.1 Total Neutron Cross-Section

The total neutron cross-section from 1.0×10^{-5} eV to 690 keV is given by the resolved resonance parameters in File 2 along with the background in File 3. From 690.0 keV to 11.0 MeV it was obtained from a spline fit to the recent data of Schwartz et. al.⁸ These are new National Bureau of Standards data obtained with a time-of-flight arrangement and a resolution which varied from 0.2 ns/m at 500 keV to 0.08 ns/m at 15.0 MeV. The accuracy of the data varies from 3-4% and the data were obtained with two sample thicknesses of 0.4047 and 1.032 atoms/barn. Further details of these measurements are to be found in this reference. On comparing these data with the measurements of Cierjacks et. al.⁹ between 11.0 and 15.0 MeV it was found that the NBS data were consistently higher than the Karlsruhe data; their difference being of the order of 75 mb at 15.0 MeV. There is also considerable statistical spread in the NBS data around 15.0 MeV. The Karlsruhe data above 6 or 7 MeV are considered reliable as they do not suffer from the counting rate and dead-time corrections as at lower energies. Hence, it was decided to use these data between 11.0 and 20.0 MeV after making a spline fit. This spline fit as plotted against the experimental data are shown in Figs. 5-11. After the evaluation of the total cross-section was finished, a set of new preliminary measurements of the total cross-section by Perey et. al.¹⁰ became available. These measurements used two sample thicknesses of approximately 0.2 and 1.0 atoms/barn. and an energy resolution (5 ns bursts and 47.35 m of flight path) which is comparable to the NBS data and slightly worse than the 1968 Karlsruhe work. On comparing these data with the NBS measurements the agreement was found to be excellent. It is hoped to include these data in a future evaluation when the final data are available.

NATURAL NICKEL

TOTAL
NEUTRON CROSS SECTION

ENDF/B MAT NO. 1190

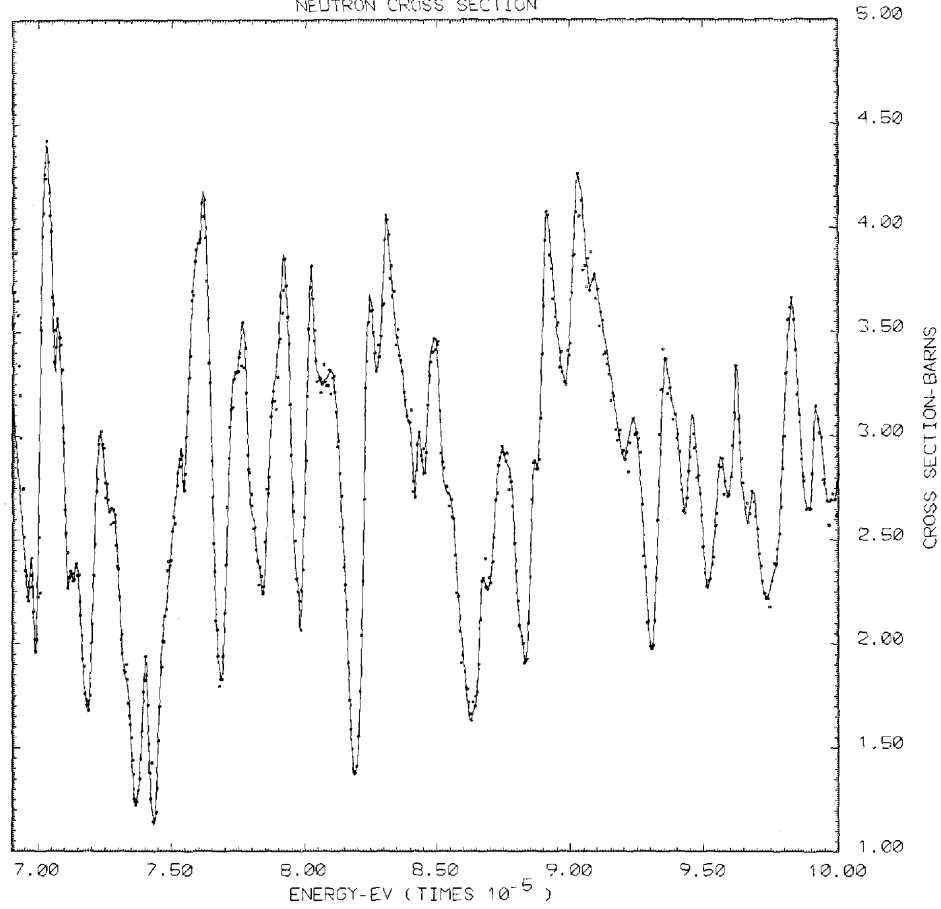


Fig. 5. Nickel Total Cross-Section 0.7 - 1.0 MeV

NATURAL NICKEL

TOTAL
NEUTRON CROSS SECTION

ENDF/B MAT NO. 1190

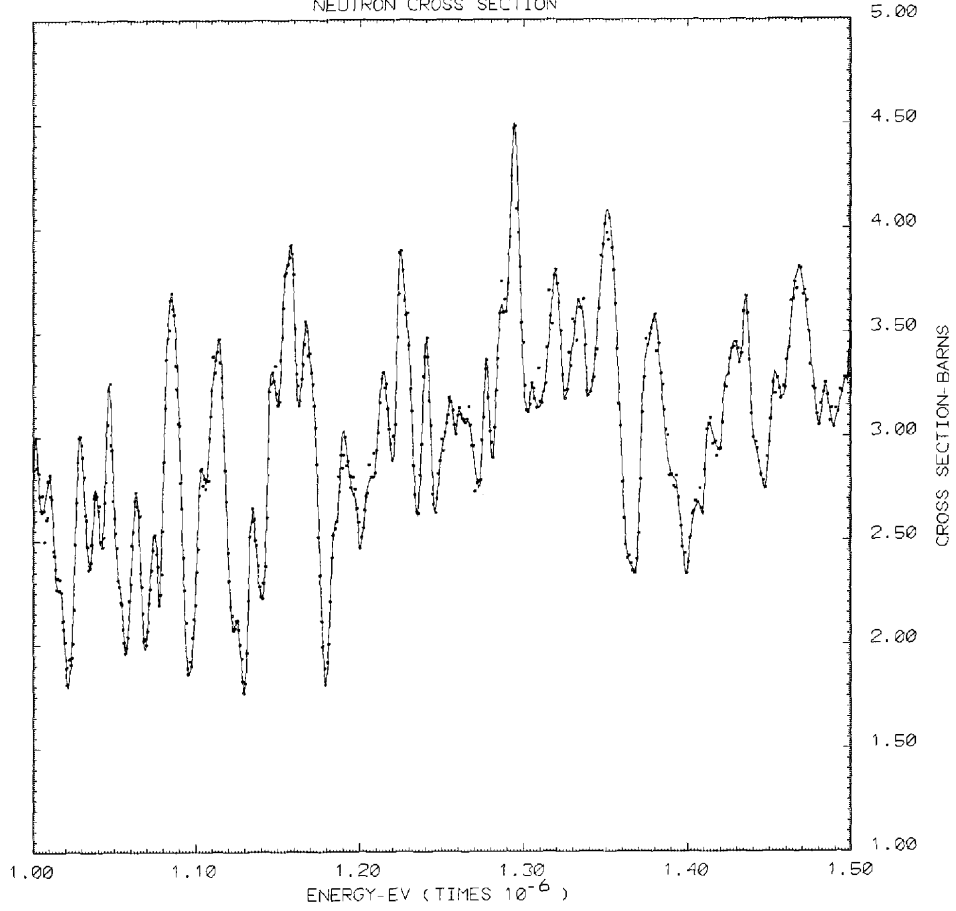


Fig. 6. Nickel Total Cross-Section 1.0 - 1.5 MeV

NATURAL NICKEL

TOTAL
NEUTRON CROSS SECTION

ENDF/B MAT NO. 1190

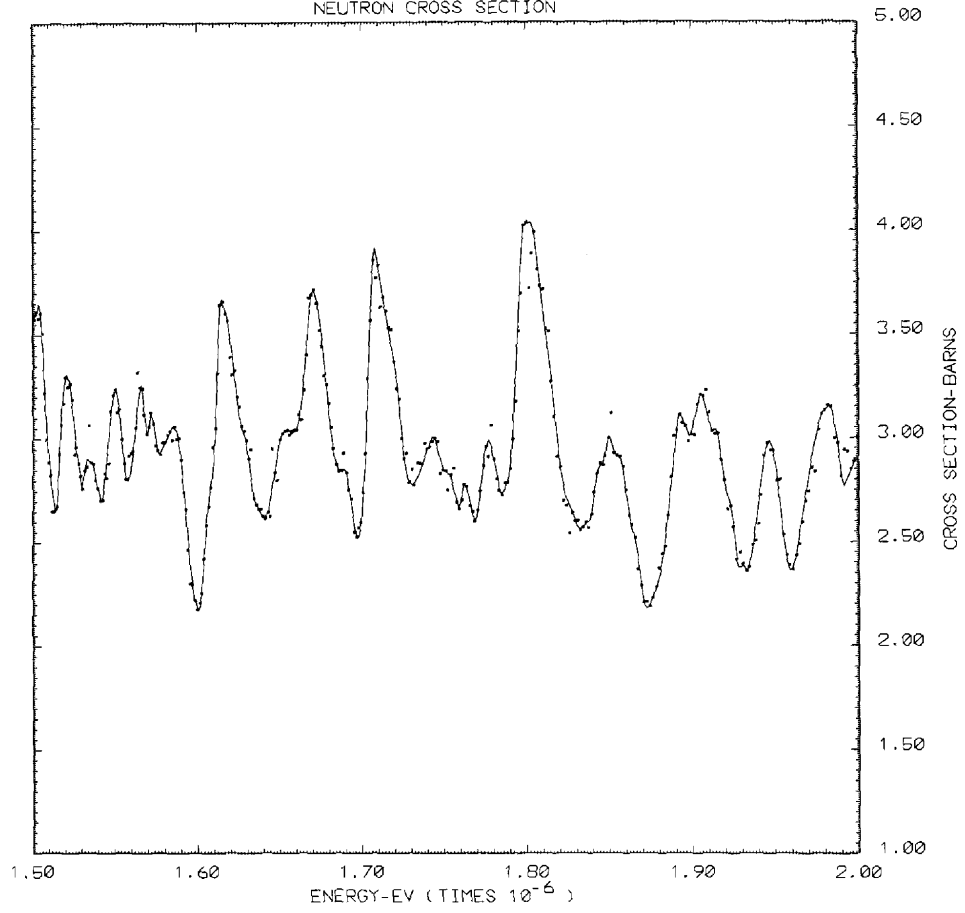


Fig. 7 . Nickel Total Cross-Section 1.5 - 2.0 MeV

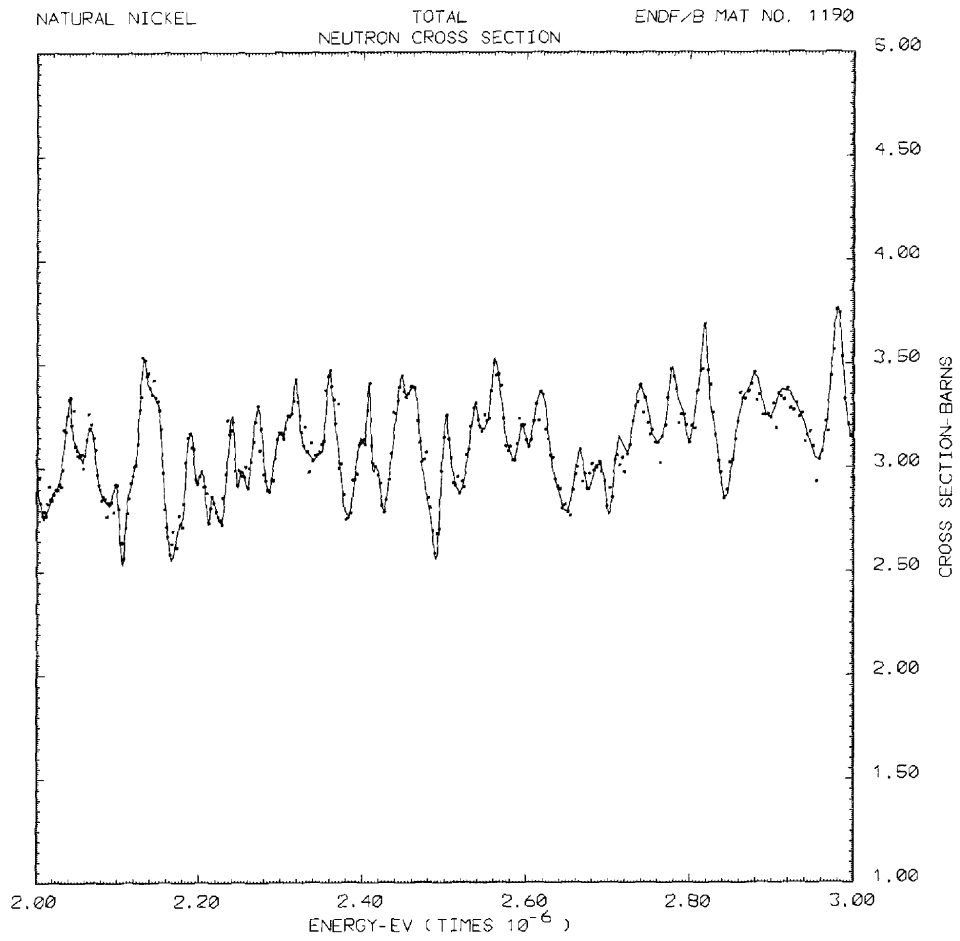


Fig. 8. Nickel Total Cross-Section 2.0 ~ 3.0 MeV

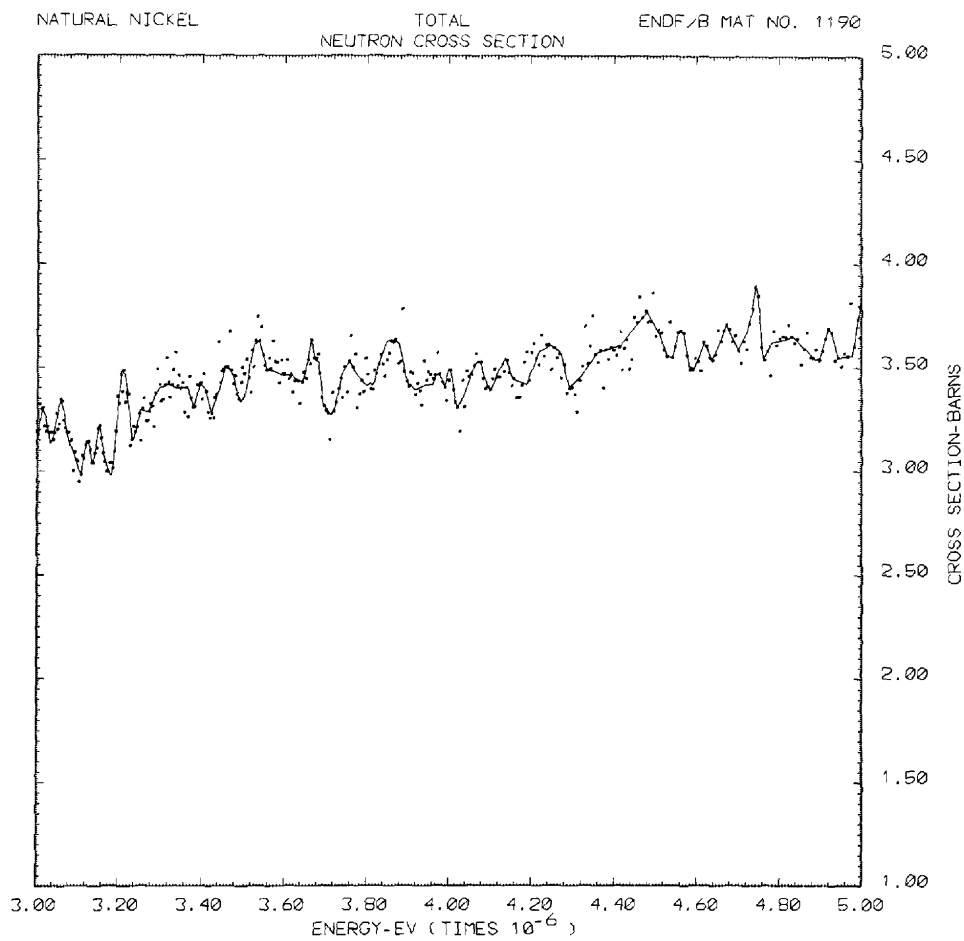


Fig. 9. Nickel Total Cross-Section 3.0 - 5.0 MeV

NATURAL NICKEL

TOTAL
NEUTRON CROSS SECTION

ENDF/B MAT NO. 1190

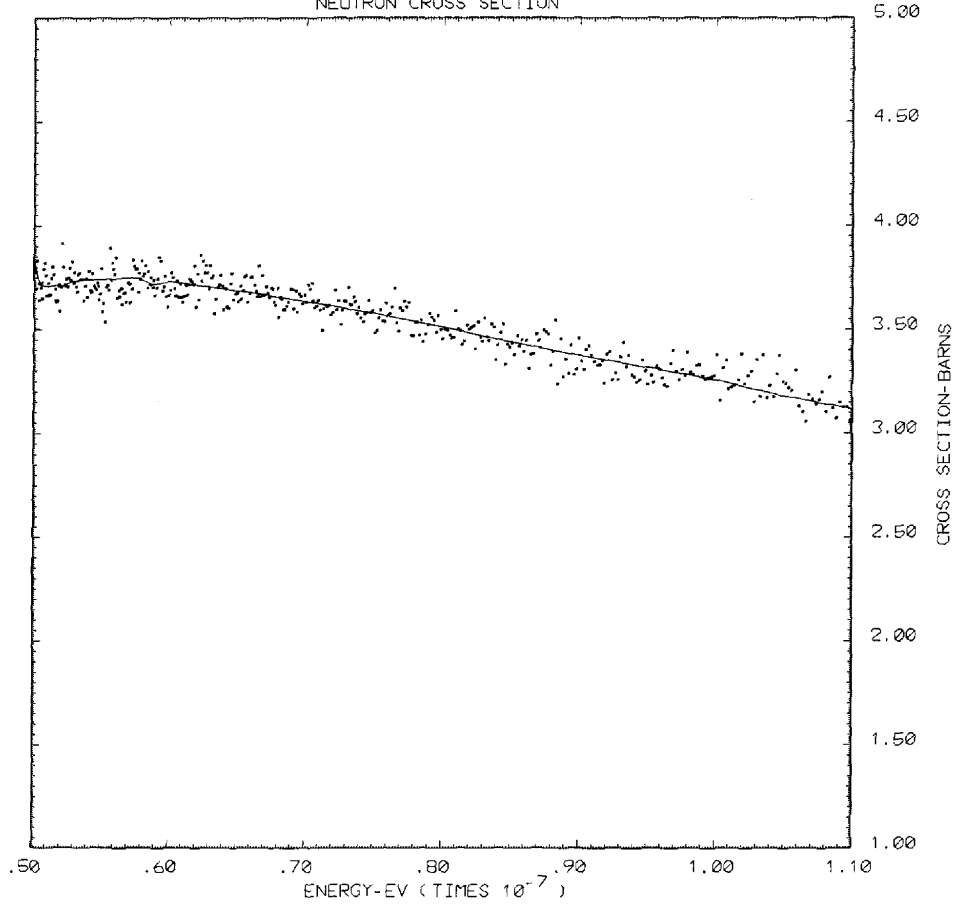


Fig. 10. Nickel Total Cross-Section 5.0 - 11.0 MeV

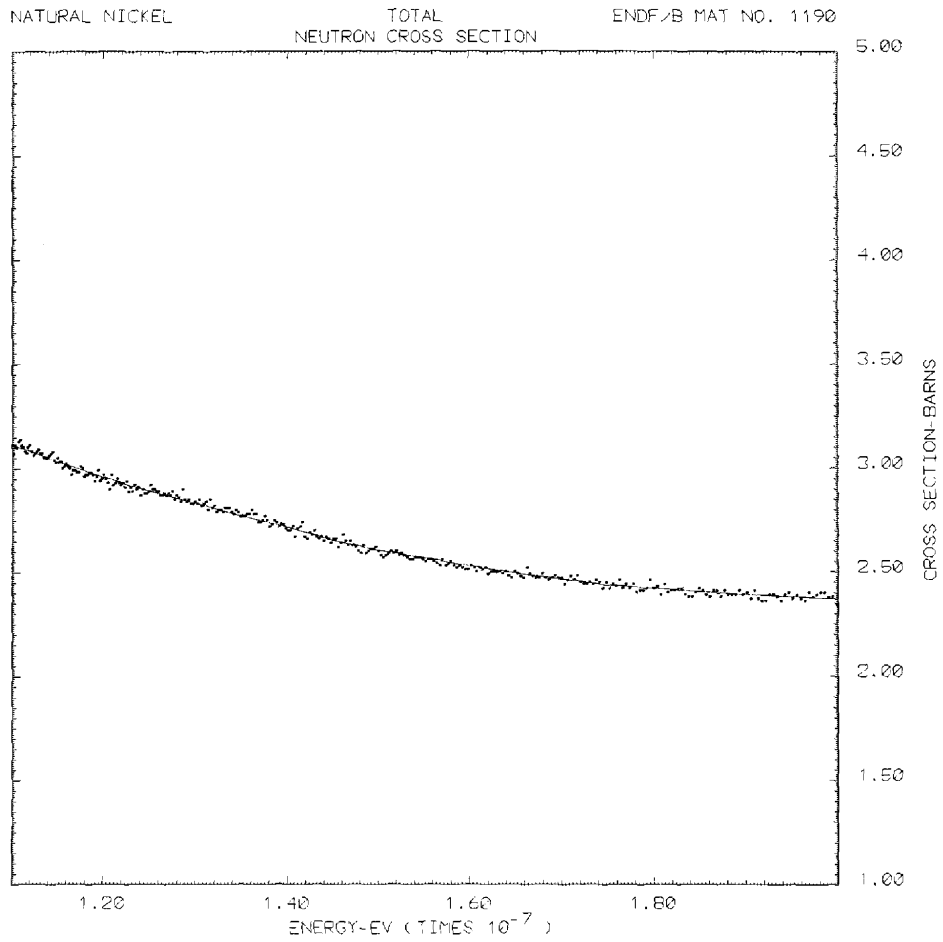


Fig. 11. Nickel Total Cross-Section 11.0 - 20.0 MeV

As is well known, the total cross-section is the easiest cross-section to measure and as such is not plagued with different data uncertainties. Apart from the thermal and resonance region where the problems of measurement and analysis are more complicated it is estimated that the total cross-section has an error of 1.5% to 3% in the MeV energy range. The thermal and resonance cross-sections are known within 5-10% accuracy. These errors are given in Table 8.

3.2 The Elastic Scattering Cross-Section

The elastic scattering cross-section from $1.0E - 05$ eV to 690.0 keV is given by the resolved resonance parameters and the File 3 background. Above this energy from 690.0 keV to 20.0 MeV it was obtained by subtracting the sum of cross-sections due to all the non-elastic processes from the total cross-section. This is shown in Figs. 12-17 plotted against the available experimental data.¹¹⁻²⁶ These data were obtained by integrating the differential elastic scattering measurements and as such suffer from the problems of such data viz. the difficulty of measurement in the forward and backward directions. These data are summarized in Table 3. It should be noted that Kinney et al.¹¹ have pointed out that the recent data of Holmqvist et al.¹² are systematically lower above 4.6 MeV and have suggested that they be increased by about 10%. Holmqvist data were therefore plotted after increasing the cross-section by 15% at 6.09 MeV and by 10% at 7.05 and 8.05 MeV. The horizontal bars associated with the data points indicate information on the energy resolution of the data where it is available and the elastic cross-section with its structure should be suitably averaged over this energy range for a meaningful comparison with the experimental values. In general, the agreement between the evaluated cross-section and the experimental data is good - though the smooth elastic

cross-section above 6.0 MeV (Fig. 17) seems to be consistently higher than the experimental data.

The errors in this cross-section are again given in Table 8. The relatively small errors quoted for it are due to the fact that it was determined by subtracting the accurately measured data on the non-elastic cross-section from the total cross-section.

3.3 The Non-Elastic Scattering Cross-Section

This cross-section represents the sum of all cross-sections of reactions other than elastic scattering. It is not given as such (MF = 3, MT = 3) in the data files as it is redundant and can easily be obtained from the other cross-sections already given. However, it is useful to plot this cross-section against the experimental data where available. Most of the results were measured using the sphere transmission method and after applying the usual corrections are bound to be more accurate than those obtained by integrating the differential elastic scattering cross-section and subtracting it from the total. These experimental data are very useful in estimating some of the partial cross-sections for the non-elastic processes for which there are no extensive experimental data as they form an upper bound to the sum of such cross-sections. The available experimental data are summarized in Table 4. It should be noted here that the results of Bauer et. al.¹⁷ and Holmqvist and Wiedling³⁴ were obtained by subtracting the integrated differential elastic scattering cross-sections. In addition, the comments on the latter data set made earlier should be kept in mind and the elastic scattering at 6.09 - 8.05 MeV should be increased by 10-15% with a corresponding decrease in the non-elastic cross-section. A plot of these data and the non-elastic cross-section obtained from the evaluated data files is shown in Fig. 18.

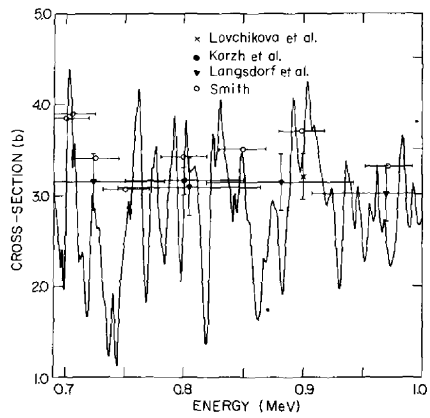


Fig. 12. Nickel Elastic Cross-Section
0.7 - 1.0 MeV

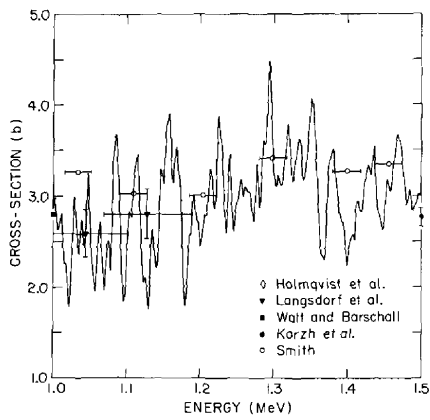


Fig. 13. Nickel Elastic Cross-Section
1.0 - 1.5 MeV

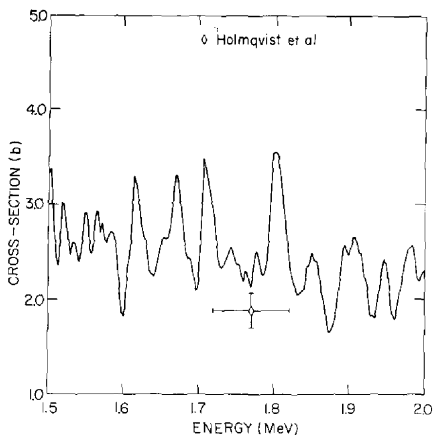


Fig. 14. Nickel Elastic Cross-Section
1.5 - 2.0 MeV

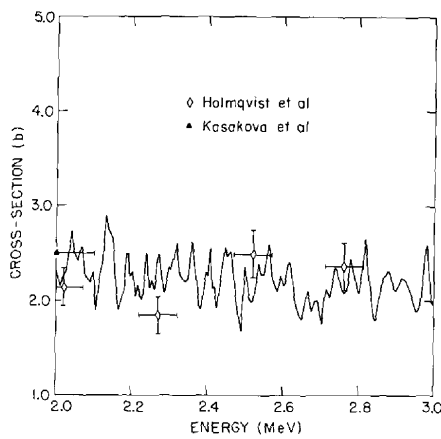


Fig. 15. Nickel Elastic Cross-Section
2.0 - 3.0 MeV

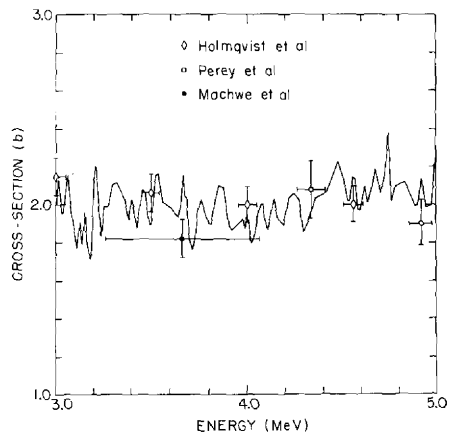


Fig. 16. Nickel Elastic Cross-Section
3.0 - 5.0 MeV

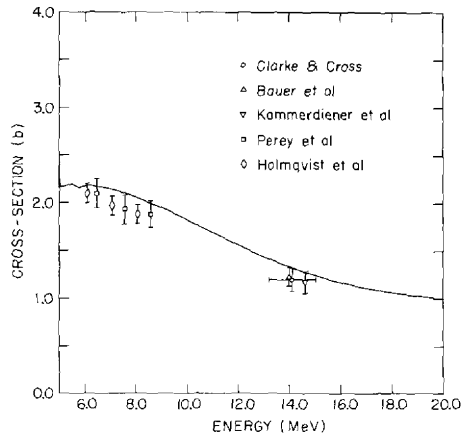


Fig. 17. Nickel Elastic Cross-Section
5.0 - 20.0 MeV

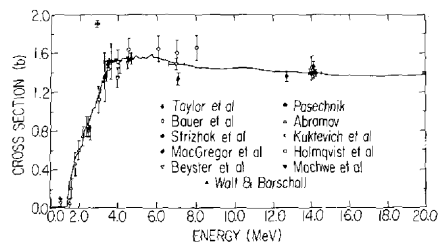


Fig. 18. Nickel Non-Elastic Cross-Section

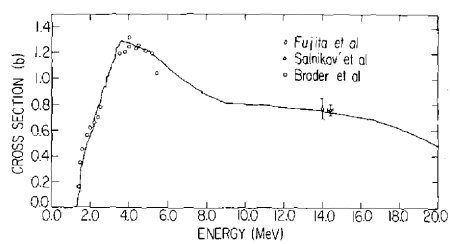


Fig. 19. Nickel Total Inelastic Cross-Section

Where the high-energy part of the cross-section is assumed to be essentially constant passing through the cluster of points at 14.0 MeV. The structure in the curve at low energies is mainly due to the (n,p) cross-section.

The errors in this cross-section appear to be of the order of 5-10% at the lower end of the energy scale and 3-5% in the 14 MeV region. Some measurements at low energies have larger errors 17-20% as can be seen from Table 4.

3.4 The Total In-elastic Scattering Cross-Section

The experimental data on the total inelastic scattering cross-section of nickel are summarized in Table 5. The data of Broder et. al.^{39,40} were obtained by measuring the inelastic gamma rays and extend from 1.4 - 5.42 MeV. In the experiments of Fujita et. al.³⁷ and Sal'nikov et. al.³⁸ the outgoing neutrons were detected with a time-of-flight arrangement to perform the energy analysis. After allowing for the contributions of other (n, particle) reactions, the total inelastic scattering cross-section was deduced. The results of these two experiments for the total in-elastic scattering cross-section are in good agreement. A plot of these data against the evaluated cross-section is shown in Fig. 19.

The errors quoted by the experimenters for the 14 MeV value are 5-10%. It is possible there are much larger errors in these due to subtraction of other (n, particle) cross-sections. Unfortunately no errors were given by Broder and the error estimates in Table 8 are based on the errors in the non-elastic and discrete in-elastic cross-sections.

3.5 In-Elastic Scattering Cross-Section to the Discrete Levels and the Continuum

The data on the inelastic scattering cross-section to the discrete excited states of the nickel isotopes were obtained either by measuring the

differential inelastic scattering cross-section or the gamma-rays produced by inelastic scattering. In the latter case the measured cross-sections have to be corrected for the contributions of the gamma-rays from the higher levels in the cascade. There are reasonably extensive data for the first excited 2+ states of ^{58}Ni , ^{60}Ni and ^{62}Ni . As the energy of excitation increases in some cases cross-sections corresponding to a group of unresolved levels have been measured and in other cases the data are in the form of gamma production cross-sections and it is not clear whether they have been corrected to give inelastic cross-section and hence, are of doubtful value. The experimental data^{11,41-49} devoid of these short-comings were used to normalize nuclear model calculations which could then be extended to the energy regions where no experimental data are available. Recently, there have been some new measurements by Smith et. al.⁵⁷ on the elastic and inelastic cross-sections of the nickel isotopes. Since the data were not available at the time of the evaluation, they were not used.

The nuclear model calculations to estimate the inelastic cross-sections were carried out using the code `COMMNUC-I`⁵⁰ which uses Hauser-Feshbach theory with width fluctuation corrections to calculate the compound nuclear contributions to the cross-sections. In these calculations, the optical model parameters obtained by Stieglitz et. al.¹ by fitting the experimental differential elastic scattering data from 0.2 to 14 MeV were used. These are given in Table 6. In addition, the level structure of the nickel isotopes in Fig. 1-4 was used. In ^{58}Ni the spin-parity assignments of the levels above 3.420 MeV are uncertain; hence it was assumed that levels at excitation energy 3.5 MeV and above could be described by a continuous distribution of levels whose level density is given by an expression of the type given by Gilbert and Cameron.⁵¹

The calculated curves as normalized to the experimental data for the 1.173 MeV, 1.332 MeV and 1.454 MeV first excited states in ^{62}Ni , ^{60}Ni and ^{58}Ni respectively are shown in Figs. 20-22. Above 9 MeV it can reasonably be assumed the compound nuclear contribution to these cross-sections is negligible and the curve was smoothly joined to the results of coupled channel calculations which give the direct reaction contribution at higher energies. These calculations were carried out using the code JPIXR⁵² which is a slightly modified version of the code JUPITOR by Tamura⁵³. The optical model parameters used in these calculations are given in Table 6. In these calculations only three levels viz: the ground state, the first excited 2+ state and either the 3- or one of the two phonon states with spin-parity 0+, 2+ or 4+ were coupled together at a time to keep the computer time within reasonable bounds. The coupling parameters used in these calculations are from the literature^{1,54-56} and were obtained from an analysis of (n,n'), (α , α') and (p,p') reactions. In these calculations, the effect of coupling the two phonon states to the ground and first excited states was found to be small hence only the results of the coupling 0+ - 2+ - 3- were used in the evaluation. The inelastic cross-section thus calculated is found to be a slowly decreasing cross-section of the order of about 40 mb at 14.0 MeV. Kammerdiener²⁶ measured the inelastic scattering cross-section to the first excited states of the nickel isotopes in natural nickel to be 39.5 ± 2.8 mb at 14.6 MeV. The results of these calculations gave 42 mb for this cross-section in good agreement with the data. This experimental value of Kammerdiener agrees with 39.4 mb obtained by integrating Stelson's data²⁶.

In addition to calculating the direct reaction excitation cross-sections to the different levels of the target nucleus, the coupled channel

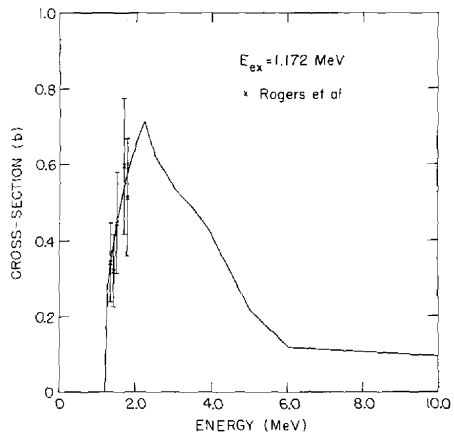


Fig. 20. Nickel Inelastic Cross-Section
 $E_{ex} = 1.172 \text{ MeV}$

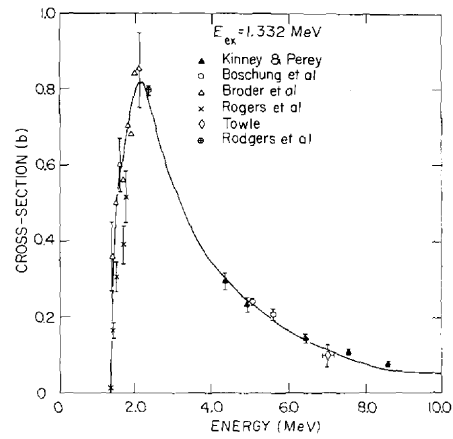


Fig. 21. Nickel Inelastic Cross-Section
 $E_{ex} = 1.332 \text{ MeV}$

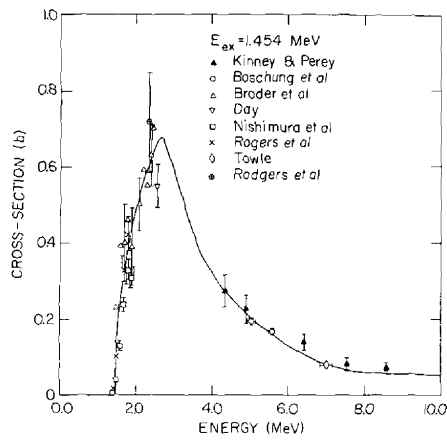


Fig. 22. Nickel Inelastic Cross-Section
 $E_{ex} = 1.454 \text{ MeV}$

calculations also enable one to fit the data on inelastic scattering to these levels and their forward peaking at higher energies. This will be discussed in a subsequent section. (4.2).

The in-elastic cross-sections to the other excited states for which there are no experimental data were obtained by normalizing the results of nuclear model calculations such that their sum along with the capture and (n, particle) reactions gave a non-elastic cross-section passing through the experimental data.

3.6 The Capture Cross-Section

The capture cross-section of nickel from 1.0×10^{-5} eV to 690 keV is given by the resonance parameters and the smooth background in File 3. Above this energy and extending up to about 1.0 MeV there are only two sets of data by Diven et. al.⁵⁸ and by Staviskii et. al.⁵⁹. The first set of data were obtained by measuring the capture events in a one meter diameter liquid scintillator tank and an energy resolution varying from 25 keV to 90 keV. Corrections were applied to take into account multiple scattering and attenuation of the neutron beam within the sample and the escape of high energy capture gamma rays from the detector by assuming an average efficiency of $95 \pm 5\%$. The cross-section was determined by using the capture plus fission cross-section of ^{235}U as the standard and a 100% efficiency for it. The quoted uncertainty in the capture cross-section of nickel at 400 ± 90 keV is about 19% (8.0 ± 1.5 mb) and the assumed capture plus fission cross-section of ^{235}U is 1500 mb which differs by about 5% from the currently accepted value of 1417 mb (Version IV ^{235}U evaluation). However, because of the large error in the measured data, they were not normalized to this value. Staviskii and Shapar⁵⁹ measured the capture cross-section of nickel from 35 keV to 1 MeV

with an energy resolution of 20 keV using a CaF_2 scintillator as the detector in an annular geometry. They then normalized their data to the 400 keV value of Diven et. al. It is estimated that the uncertainty in their measurements is of the order of 15%. A plot of these two sets of measurements in the region 690 keV to 1 MeV along with the capture cross-section in the evaluated data files is shown in Fig. 23. This cross-section was calculated using the code COMMNUC-I and the parameter $2\pi \langle \Gamma_\gamma \rangle / \langle D \rangle$ (where $\langle \Gamma_\gamma \rangle$ is the gamma width and $\langle D \rangle$ is the average level spacing) was adjusted so that the calculated curve would pass through the measured data points. The curve shown corresponds to the following values of this parameter: $^{58}\text{Ni} = 2.67 \times 10^{-4}$, $^{60}\text{Ni} = 2.60 \times 10^{-4}$, $^{62}\text{Ni} = 2.22 \times 10^{-4}$, $^{64}\text{Ni} = 2.02 \times 10^{-4}$. Except for ^{64}Ni , these are low compared to the values one obtains for this parameter from the resolved resonance data. These are: $^{58}\text{Ni} = 1.01 \times 10^{-3}$, $^{60}\text{Ni} = 6.16 \times 10^{-4}$, $^{62}\text{Ni} = 3.09 \times 10^{-4}$ and $^{64}\text{Ni} = 2.02 \times 10^{-4}$. Since the calculated capture cross-sections with these parameters were too high compared to the experimental data; $2\pi \langle \Gamma_\gamma \rangle / \langle D \rangle$ was lowered in value to agree with the experimental data. Further measurements of the capture cross-section over a wider energy range and with improved accuracy are therefore indicated to improve our knowledge of this cross-section. The calculated capture cross-section at 11.0 MeV was found to be 0.1 mb and it was set equal to zero from 12.0 to 20.0 MeV.

It is estimated that the error in the thermal capture cross-section of nickel is about 4% by looking at the experimental data.⁶⁰ The error in the resolved resonance region appears to be between 15-25% and above 690 keV about 20% considering that the data uncertainty in Divens data at 400 keV is 19%.

The Q-value given for the capture reaction viz: 8.6 MeV is an effective Q-value defined by $\bar{B}_n = \frac{\sum B_{ni} a_i \sigma_{n\gamma i}}{\sum a_i \sigma_{n\gamma i}}$ where the summation is over the nickel isotopes, a_i are their abundances and $\sigma_{n\gamma i}$ are thermal capture cross-sections as given in Ref. 60 and B_{ni} are the Q-values for capture given in Table 2.

3.7 The (n,2n) Cross-Section

There are very few measurements of the (n,2n) cross-section of the natural element. One of them is by Benveniste⁶¹ at 14 MeV and the other by Sal'nikov et. al.³⁸ at $14.4 \pm .14$ MeV. Benveniste measured the (n,2n) cross-section using a 40 inch cadmium loaded liquid scintillator to obtain an (n,2n) cross-section of 200 ± 20 mb. Sal'nikov et. al. measured the spectra and the differential cross-section of neutrons by the time-of-flight method. The neutrons were detected with a liquid scintillation detector with a neutron recording threshold of 100 keV. The result of this experiment is to give $\sigma(n,2n) + \sigma(n,pn') = 230 \pm 20$ mb. Unfortunately because of a lack of knowledge of the $\sigma(n,pn')$ cross-section and the problems of estimating it, this result is not of much help in fixing the (n,2n) cross-section in the vicinity of 14 MeV. One could perhaps conclude that 200 mb represents an upper limit to this cross-section at 14.0 MeV.

The above two experiments detect the out-going neutrons as opposed to the more popular activation method for measuring the (n,2n) cross-sections. In the case of the nickel isotopes, the (n,2n) reaction leads to an unstable final nucleus only in the case of ^{58}Ni . Hence, though there are extensive data on the (n,2n) cross-section of ^{58}Ni there are none for the other isotopes. Therefore, an indirect method of estimating this cross-section had to be adopted for the rest of the isotopes. This will be described below after discussing the status of the ^{58}Ni (n,2n) cross-section data first.

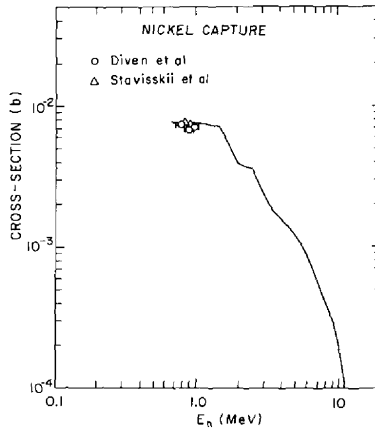


Fig. 23. Capture Cross-Section of Nickel

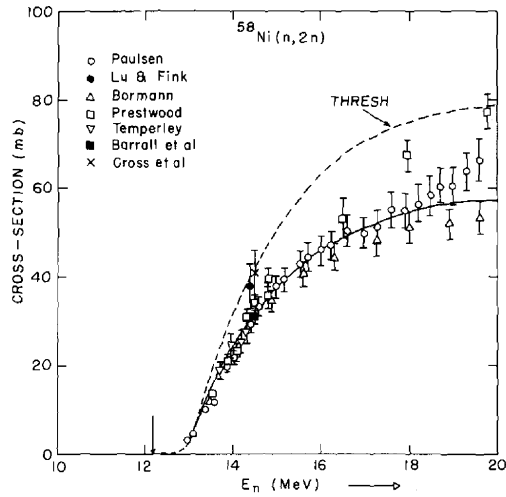


Fig. 24. $^{58}\text{Ni} (n,2n)$ Cross-Section

There are extensive data on the (n,2n) cross-section of ^{58}Ni from its threshold of 12.415 MeV to 20 MeV. The most extensive data covering a wide range are by Paulsen and Liskien⁶² and by Bormann et. al.⁶³. Paulsen determined the (n,2n) cross-section from 12.98 to 19.6 MeV by the activation method and the measurement of the annihilation radiation with an accuracy of about 7%. The activation experiments of Bormann measured the gamma and positron activities with a NaI(Tl) detector and a γ - γ coincidence spectrometer and have a comparable accuracy and extend from 12.95 to 19.6 MeV. As can be seen from Fig. 24, though these two sets of data are in good agreement with one another below 16 MeV, they diverge above this energy with the Paulsen data being larger than the other set by as much as 12% or approximately two standard deviations. There are two other data sets which extend up to 20.0 MeV: one by Prestwood and Bayhurst⁶⁴ and the other by Jeronymo et. al.⁶⁵. Prestwood and Bayhurst counted the ^{57}Ni β particles and used ^{238}U fission cross-sections to monitor the neutron flux. These data agree with the general trend of other measurements up to about 14.0 MeV; above this energy they are higher giving 77.4 mb at 19.8 MeV. These cross-sections were considered too high and were not included in the evaluation. The Jeronymo data obtained by measuring the gamma rays following the decay of ^{57}Ni give a cross-section of about 40 mb at 20 MeV and are considered too low to merit consideration (not shown in Fig. 24). The data of Lu and Fink⁶⁶ at 14.4 MeV and Cross et. al.⁶⁷ at 14.5 MeV are higher than other data at this energy. The data of Csikai⁶⁸ (not shown) between 13.56 and 14.71 MeV appear to be higher than other measurements and also show a peculiar trend at variance with other experiments (see the plot in Ref. 69 p. 28-58-4) and were not considered in the evaluation. Other data sets shown in the plot are by Temperley⁷⁰ and

by Barrall et. al.^{71,72,73}. Temperley measured the annihilation radiation from the decay of ⁵⁷Ni and the data are in good agreement with other measurements in the energy region 13.72 to 14.79 MeV. Barrall and co-workers obtained 30.9 ± 2.0 mb at $14.5 \pm .2$ MeV, 33.4 ± 2.0 mb at $14.6 \pm .12$ MeV and 36.0 ± 3.0 mb at 14.8 MeV in good agreement with other data sets. Rayburn⁷⁴ measured the (n,2n) cross-section as 34.2 ± 2.6 mb at $14.4 \pm .3$ MeV based on ⁶³Cu (n,2n) = 503 mb. In the ENDF/B-III MAT = 1085 evaluation this cross-section is found to be 533 mb. Therefore, a renormalized value of 36.2 ± 2.7 mb is obtained which is slightly higher than other data at this energy. Preiss and Fink⁷⁵ obtained 52 ± 5 mb at $14.8 \pm .9$ MeV using ⁶³Cu (n,2n) = 556 mb as the standard cross-section; this value appears to be too high. Bramlett and Fink⁷⁶ obtain 31.6 ± 4.0 mb at $14.7 \pm .2$ after their value is renormalized to ²⁷Al (n, α) = 116.1 mb, and is a little on the low side. In addition, Glover and Weigold's⁷⁷ measurements follow the general trend of other data except for the last two points at 14.77 MeV and 14.88 MeV. Some of these data were not plotted in Fig. 24 for fear of cluttering up the diagram. After considering all these data, a smooth curve was drawn through these data points with the curve following the general trend of the Bormann data at higher energies and lying lower than the Paulsen measurements and higher than the Bormann data. In Fig. 24 the dashed line shows the (n,2n) cross-section as calculated using the code THRESH⁷⁸ which uses systematics of nuclear data to calculate the various (n,particle) cross-sections. Ratios of these two curves were determined as a function of energy from the threshold to 20.0 MeV. These were found to be essentially constant with an average of 0.74 and the maximum value differing from the minimum by only 10%. Hence, THRESH calculations were carried out for the other nickel isotopes for which there are no

data; and the calculated cross-sections were reduced by this factor to give the isotopic (n,2n) cross-sections. These were weighted with the isotopic abundance to give the cross-section in the evaluated data files. This is shown in Fig. 25. It is interesting to compare the result thus obtained with an estimate of the (n,2n) cross-section using the experimental data for neighboring nuclei and N-Z systematics by Bödy and Csikai⁷⁹. They obtain for $\sigma(n,2n)$ at 14.7 MeV a value of 183 ± 15 mb and the present evaluation gives 161 mb in good agreement with their estimate. These are to be compared with data of Sal'nikov et. al.³⁸ who measured $\sigma(n,2n) + \sigma(n,pn) = 230 \pm 20$ mb for natural nickel at 14.4 MeV.

After examining all the experimental data, their disagreement at higher energies and the procedures that had to be adopted because of lack of data for isotopes other than ^{58}Ni an error estimate of 15% for this cross-section appears to be conservative.

3.8 The (n,p) Cross-Section

The (n,p) cross-section measurements on natural nickel are mostly around 14 MeV. Further, those that have involved the detection of outgoing protons have been plagued with problems of (n,n'p) contamination (Hassler and Peck⁸⁰) or were measured with a high threshold for proton detection (Verbinski et. al.⁸¹) or have given rather large values of the cross-sections⁸². On the other hand, the data on the most abundant isotopes ^{58}Ni and ^{60}Ni obtained by activation analysis are extensive, complete and consistent. Hence, it was decided to evaluate the (n,p) cross-section for the element in terms of the cross-sections of the individual isotopes.

The data on ^{58}Ni (n,p) cross-section is extensive and of good quality with the result that this reaction is used in dosimetry applications.

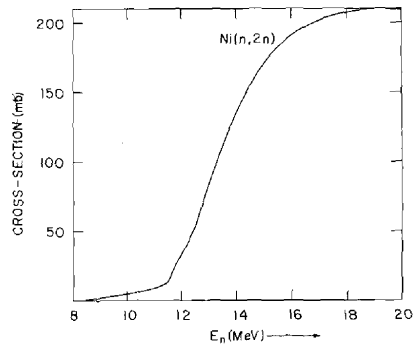


Fig. 25. Ni(n,2n) Cross-Section

In the Dosimetry Data Library which is part of the ENDF/B-IV data library, the ^{58}Ni (n,p) evaluation is by R.E. Schenter⁸³. It was decided to adopt this evaluation for the sake of consistency and a detailed discussion of this evaluation will be published⁸³. The data sets on which this evaluation is based are also listed in the File 1 comments of this data file (MAT-6419).

The most extensive data on the ^{60}Ni (n,p) cross-section from 5.76 to 19.55 MeV are by Paulsen and Liskien.⁸⁴⁻⁸⁷ In these experiments the induced activity was measured by γ - γ coincidence counting and the efficiency of the coincidence spectrometer determined from calibrated radioactive sources whose activity was known to $\pm 0.5\%$. The errors in these data vary from 7-10% except for a few points where they are larger, up to 16%. The measurements of Cross et. al.⁸⁸ at 14.5 MeV when renormalized to an ^{27}Al (n, α) cross-section of 118.6 mb (MAT = 1135 ENDF/B-III) obtain 186 mb and a later⁸⁹ result by the same authors is 165 mb: both appear to be too high compared to the Paulsen and Liskien data. Allan⁹⁰ determined the (n,p) cross-section by measuring it at 120° to the neutron beam using photographic emulsion plates and multiplying by 4π the observed differential cross-section. He obtained a value of 134 ± 9 mb at 14 MeV in good agreement with Liskien and Paulsen. However, this technique has given results widely at variance with others. Storey et. al.⁹¹ have determined the (n,p) cross-section to be 158 ± 32 mb at 14.1 MeV which appears to be rather high compared to the general trend of the other data. Hemingway⁹² obtained a cross-section of 129 ± 16 mb at $14.7 \pm .2$ MeV using ^{56}Fe (n,p) $^{56}\text{Mn} = 97.8$ mb as a standard. This is to be compared with 104 mb recommended for the standard in the evaluation (MAT-6410) in ENDF/B-IV dosimetry files. This implies a 6% upward renormalization of the Hemingway value to give 137 mb. Levkovskii et. al.⁹³ have measured the

(n,p) cross-section to be 130 ± 40 mb which again is higher than the general trend of the Liskien - Paulsen data. The data not considered in this evaluation are by Preiss et. al.⁷⁵ (cross-section to metastable state only) March et. al.⁹⁴ (too low) Allan⁹⁵ (highly discrepant). In looking at all the available data it is unfortunate that there are no data from the threshold energy to 5.75 MeV. Hence, the rising part of the curve was drawn similar to the ^{58}Ni (n,p) cross-section curve after suitably shifting it for differences in the Q-values and smoothly joined to a curve drawn through the experimental data at higher energies. The trend of the curve in this energy region is mainly determined by the Paulsen and Liskien data. This is shown in Fig. 26.

The data on the remaining stable isotopes of nickel are rather sparse. For ^{61}Ni Cross et. al.⁸⁹ obtained 83 ± 8 mb at 14.5 MeV with ^{27}Al (n, α) = 115 mb as the standard. If one renormalizes the cross-section to 118.6 mb recommended in ENDF/B-III evaluation, (MAT = 1135) one obtains 86 ± 8 mb. There is a low energy point by VanLoeff⁹⁶ at $3.3 \pm .1$ MeV which renormalized to ^{58}Ni (n,p) cross-section recommended by Schenter⁸³ gives 4.4 ± 1.5 mb. Valter et. al.⁹⁷ obtain an experimental result at 14.1 MeV which when normalized to the ENDF/B-III aluminum evaluation (MAT No. = 1135, ENDF/B-III) gives ^{61}Ni (n,p) = 93 ± 3 mb. In addition, there is an absolute measurement by Levkovskii et. al.⁹³ who obtain ^{61}Ni (n,p) = 98 ± 10 mb at 14.8 MeV. These data are shown in Fig. 27. The continuous curve shows the cross-section calculated by the Code THRESH without any renormalization. The good agreement may be fortuitous. The values given by this curve were taken to give the ^{61}Ni (n,p) cross-section.

The ^{62}Ni (n,p) data are shown in Fig. 28. Valter et. al.⁹⁷ determined this cross-section to be 56 ± 3 mb at 14.1 MeV with ^{27}Al (n, α) = 114 mb as the standard. If this is renormalized to a value of 123 mb (MAT-1135, ENDF/B-III) the cross-section is found to be 60 ± 3 mb which is much higher than other data in this energy region. Similarly, the datum of Cross et. al.⁸⁹ when renormalized is found to be 40 ± 6 mb at 14.5 MeV. The measurements Preiss and Fink⁷⁵ at $14.8 \pm .9$ MeV appear to be too low (4.8 mb) to merit consideration. In addition, Bormann et. al.⁶³ obtain 29.4 ± 3 mb at $14.1 \pm .15$ MeV and Levkovskii et. al.⁹³ found this cross-section to be 44 ± 5 mb at 14.8 MeV by an absolute measurement. All these data, along with the THRESH calculation are shown in Fig. 28. In view of the sparsity of experimental data and their considerable spread, it was decided to accept this curve as indicating the ^{62}Ni (n,p) cross-section.

There seem to be only two measurements of ^{64}Ni (n,p) cross-section. One is by Valter et. al.⁹⁷ which used ^{27}Al (n, α) = 114 mb as standard at 14.1 MeV. After renormalization to a standard cross-section of 123 mb it is found to be 5.4 ± 1 mb. The other measurement is by Preiss and Fink⁷⁵ who obtain $4.5 \pm .1$ mb at 14.5 MeV. The THRESH curve was therefore normalized to 5 mb at 14.5 MeV to calculate the ^{64}Ni contribution to the (n,p) cross-section.

The isotopic (n,p) cross-sections were weighted with their natural abundance to give the cross-section for natural nickel. This curve is shown in Fig. 29. The structure shown on the rising part of the curve is due to ^{58}Ni and is based on the Schenter evaluation of the (n,p) cross-section. The fission spectrum (T = 1.32 MeV) average of the evaluated (n,p) cross-section for nickel is found to be 70.1 mb.

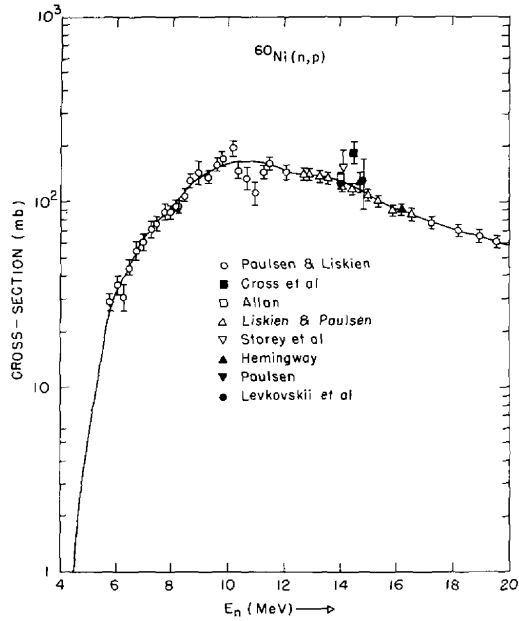


Fig. 26. $^{60}\text{Ni}(n,p)$ Cross-Section

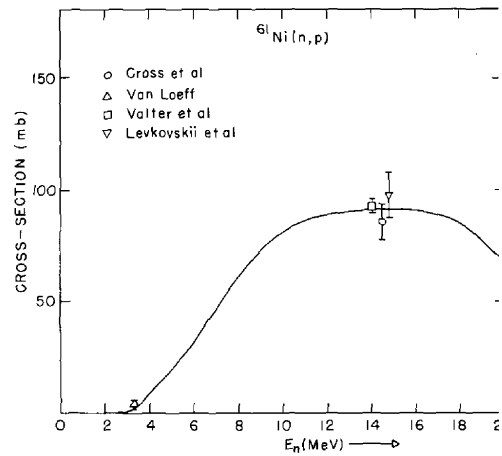


Fig. 27. $^{61}\text{Ni}(n,p)$ Cross-Section

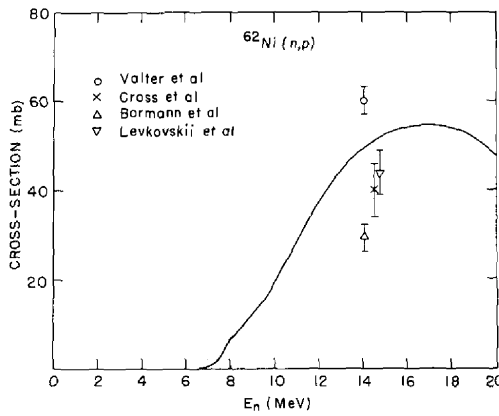


Fig. 28. $^{62}\text{Ni}(n,p)$ Cross-Section

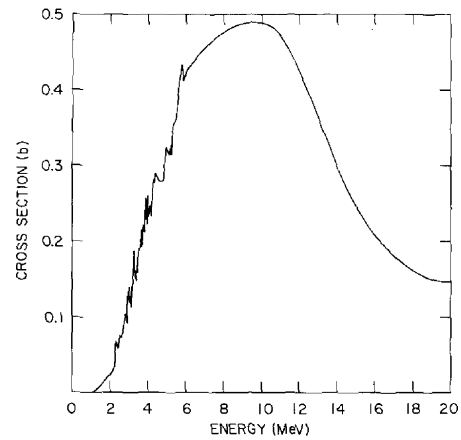


Fig. 29. Ni(n,p) Cross-Section

3.9 The (n, α) Cross-Section

The differential data on this cross-section are very meager. Seebeck and Bormann⁹⁸ obtained an upper limit for the ^{58}Ni (n, α) ^{55}Fe cross-section to be 113 ± 16 mb at 14.1 MeV. Khan et. al.⁹⁹ estimate for ^{58}Ni the (n, α) + (n, α n') + (n,n' α) cross-section to be 180 ± 20 mb at 14.7 MeV. Slinn and Robson¹⁰⁰ measured only the partial ^{58}Ni (n, α) cross-section corresponding to transitions to the ground state of the final nucleus. There are one set of data on $^{58,60}\text{Ni}$ by Spira et. al.¹⁰¹ and they also measured transitions to the ground state or a group of levels near the ground state and give only the partial cross-sections. Levkovskii et. al.¹⁰² have determined the ^{62}Ni (n, α) and ^{64}Ni (n, α) cross-sections to be 17 ± 4 mb and 5.2 ± 1.2 mb respectively at 14.8 MeV using activation analysis. Also, Yu and Gardner¹⁰³ have measured the ^{62}Ni (n, α) cross-section to be 22 ± 3 mb at 14.1 MeV.

Because of the scanty differential (n, α) data available on the nickel isotopes, it was decided to use the measured fission spectrum average of the (n, α) cross-section. In the three integral measurements described below, the total helium production is measured and as such the measured value is to be considered as a spectrum average over (n, α) + (n,n' α) + (n, α n') cross-sections and separation of the experimental value into its constituents appears to be difficult with the currently available data. However, because of the 8-9 MeV difference in the Q-values of the (n, α) and (n,n' α) reactions most of the contribution would be from the first reaction. Freeman et. al.¹⁰⁴ using a combination of vacuum fusion extraction and mass spectrometry determined the fission spectrum average to be 4.7 ± 0.6 mb. The samples were irradiated in a reactor and after applying corrections for the departure of the reactor neutron spectrum from the fission shape and using the $^{54}\text{Fe}(n,p)$ ^{54}Mn

and ^{58}Ni (n,p) ^{58}Co fission spectrum averages to be 71 ± 5 mb and 109 ± 10 mb respectively, they could obtain a corresponding average for the Ni (n, α) reaction. Their value is in excellent agreement with the data of Weitman et. al.¹⁰⁵ who obtained 4.73 mb assuming the ^{58}Ni (n,p) fission spectrum average to be 110 mb. Using ^{46}Ti (n,p) and ^{63}Cu (n, α) as standards they obtain slightly higher values of 4.83 mb and 4.98 mb respectively giving a mean value for the element as 4.84 mb. Farrar et. al.¹⁰⁶ carried out similar integral measurements on the separated stable isotopes of nickel using a high sensitivity gas mass-spectrometer system to measure the helium released. Their fission spectrum averaged (n, α) cross-sections for the individual isotopes are ^{58}Ni : 6.06 mb; ^{60}Ni : 1.12 mb ^{61}Ni : 1.83 mb ^{62}Ni : 0.097 mb and ^{64}Ni : 0.108 mb. Using these values and the natural abundance of isotopes according to Holden² the fission spectrum averaged (n, α) cross-section for nickel is found to be 4.61 mb (preliminary). Farrar claims an uncertainty of 3% in this value with error in the flux determination of 8%.¹⁰⁷ The ^{58}Ni (n,p) spectrum average used in this work appears to be 102.8 mb¹⁰⁷ and if this is renormalized to 110 mb the spectrum average is found to be 4.93 mb with 10% error. This is in good agreement with the previous two measurements.

The THRESH code in addition to generating different (n,particle) cross-sections also calculates fission spectrum averages. The normalization and the relative reactions of the (n, α) cross-sections generated for the different nickel isotopes were changed until the fission spectrum averages for (n, α) cross-section as given by Farrar were obtained. These were then weighted with the isotopic abundance to give the curve in the evaluated data files. This is shown in Fig. 30. The cross-section thus obtained at 14 MeV is 146 mb which should be compared with 180 mb measured by Khan et. al. for ^{58}Ni at 14 MeV.

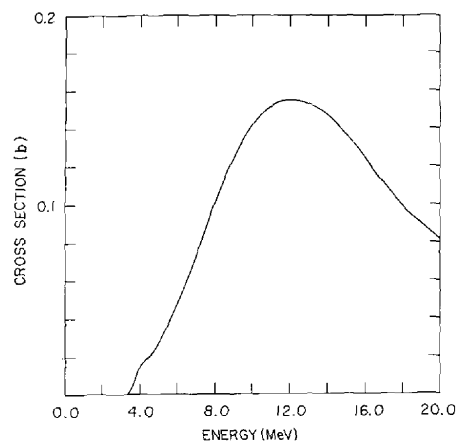


Fig. 30. Ni (n, α) Cross-Section

In arriving at this cross-section, the only condition imposed on it has been to obtain the experimentally measured fission spectrum average. Hence, it is difficult to quote any errors for it; however, in Table 8 a 20% has been quoted (the error in integral data are 10-12%) as a conservative estimate.

3.10 The (n,n'p) Cross-Section

In this section, the experimental data on the (n,n'p), (n,pn') and or (n,d) reaction cross-sections for the natural element as well as the separated isotopes will be described. In addition, the problem of reconciling these data with measurements on the non-elastic and total inelastic cross-sections at high energies will be discussed.

Hassler and Peck⁸⁰ used a counter telescope and a scintillation spectrometer to determine the (n,n'p) cross-section for natural nickel as 240 ± 50 mb at 14.4 MeV. They detected outgoing protons above an energy of 1.5 MeV. Apart from this one measurement there are no other data of the (n,n'p) or (n,d) cross-sections of natural nickel.

The experimental data on the (n,n'p) (n,pn') and (n,d) reactions or a sum of these for the nickel isotopes are summarized in Table 7. It is obvious that the measurements made by using the activation method are bound to give a cross-section which is the sum of $\sigma(n,n'p) + \sigma(n,pn') + \sigma(n,d)$ unless special efforts have been made to separate one or more of them. In these Tables some data like those of Jeronymo et. al.⁶⁵ and Purser et. al.¹¹³ have been left out as they appear to be too low to merit consideration. From these Tables one notices that the $\sigma(n,n'p) + \sigma(n,pn') + \sigma(n,d)$ cross-section for ⁵⁸Ni in the 14 MeV region varies from about 500 mb to 750 mb with an average around 600 mb. For ⁶⁰Ni it is about 50 mb; though the data on ⁶⁰Ni

are not as reliable as those on ^{58}Ni . This would indicate a cross-section for the element of the order of 420 mb. However, the $\sigma_{\text{non-elastic}} = 1.396 \text{ b}$ and the sum of $\sigma_{n,2n} + \sigma_{np} + \sigma_{na} = 580 \text{ mb}$; leaving 816 mb to be divided amongst $\sigma_{\text{total}}(n,n')$ and $\sigma(n,n'p) + \sigma(n,pn') + \sigma(n,d)$ reactions assuming that the contributions of the other (n,particle) cross-sections are negligible. The total in-elastic cross-section at $14.4 \pm .14$ measured by Sal'nikov et al.³⁸ is $760 \pm 40 \text{ mb}$ in excellent agreement with the data of Fujita et. al.³⁷ who obtained $766 \pm 78 \text{ mb}$. Both these measurements were made with a time-of-flight arrangement and by detecting the outgoing neutrons. This is to be compared with the total inelastic cross-section data of Jönsson et. al.¹¹⁴ at 15 MeV. They detected the gamma rays due to inelastic scattering to determine the cross-section. Their data are ^{58}Ni : $360 \pm 60 \text{ mb}$, ^{60}Ni : $880 \pm 130 \text{ mb}$, ^{62}Ni : 940 ± 240 . From these data the total inelastic scattering cross-section for nickel at 15 MeV is 509 mb; substantially lower than the two previous measurements. The two sets of data which look at the outgoing neutrons have the problem of separating out the contributions of other (n,particle) reactions whereas the γ -ray measurements have to be corrected for cascade contributions and other effects and are perhaps less reliable. If the total in-elastic cross-section at 14 MeV is accepted to be 760 mb then there is the problem of reconciling this cross-section with a rather high value for $\sigma(nn'p) + \sigma(n,pn') + \sigma(n,d)$ so that their sum comes out to be 816 mb. This is a situation which should be clarified with further work on these cross-sections and also more detailed measurements on the (n,n'p), (n,pn') and (n,d) cross-sections and their energy variation. In the present evaluation it was decided to accept a cross-section of 760 mb for the total inelastic cross-section at 14 MeV and assign the difference (56 mb) to the (n,n'p) + (n,pn')

+ (n,d) cross-sections. Perhaps this represents an overestimate of the (n,n') cross-sections and is definitely an underestimate of the (n,n'p) + (n,pn') + (n,d) cross-sections as indicated by the activation data. The latter cross-section as calculated by the code THRESH was normalized to 56 mb at 14 MeV and put in the data files as MT=28.

Because of the above difficulties with the experimental data it is felt that this evaluated cross-section is highly unreliable. The errors in this cross-section are put as 200% in Table 8; perhaps it is off by a much larger factor.

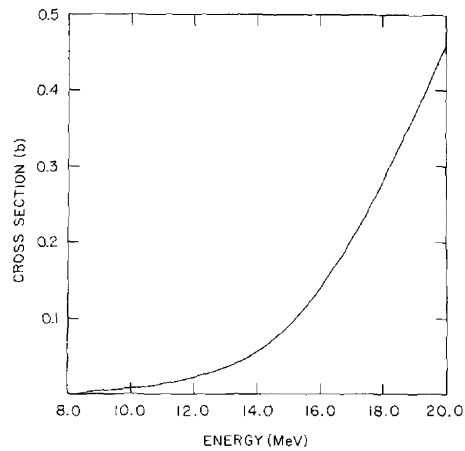


Fig. 31. Ni (n,n'p) Cross-Section

4. The Angular Distribution of Secondary Neutrons

In this section, the treatment of the elastically and inelastically scattered neutrons from nickel and its isotopes is discussed and the procedures adopted for the analysis of the experimental data are described.

4.1 Elastic Angular Distributions

The experimental data on the angular distribution of elastically scattered neutrons from natural nickel are quite extensive. Some of these¹¹⁻²⁶ have been mentioned earlier in the discussion of the data on elastic cross-section. In addition, there are a few data sets¹¹⁵⁻¹²² in the energy region less than 8.56 MeV. Above 8.56 MeV there are a few measurements^{15,17,54,26,122} around 14 MeV. The optical model parameters given in Table 6 were derived by a search procedure using this available differential elastic scattering data¹. Using these parameters and the Code¹²³ ABACUS-2 the differential elastic scattering cross-sections were calculated at those energies where there are experimental data. These calculations were then used to determine the general shape of the differential cross-sections in the backward directions (usually beyond 140° or 150° in the c-of-m system) where no experimental data are available. These values, the experimental data and the extrapolated angular distribution in the forward direction were fed into the code CHAD¹²⁴ to fit them in terms of a series of the form (in the c-of-m):

$$\frac{d\sigma}{d\omega} = \frac{\sigma_s}{4\pi} \sum_{l=0}^n (2l+1) f_l P_l(\mu)$$

to determine the coefficients f_l of the Legendre polynomials. The number n of the polynomials used was kept equal to the maximum l -value used in the code ABACUS-2 to calculate differential elastic cross-sections. It was also

verified that the fits to the experimental data satisfied Wick's inequality; the Wick's limit being determined from the spline fit to the total cross-section. In making these fits some of the low energy data of Langsdorf et. al., Cox and Korzh were combined together. In addition, some of the data sets^{117, 118, 119, 16} were not used either because their normalization or general shape did not look good or there were better and more recent data sets at the same energy. Also some data^{120, 121} could not be used as they involved measurements at only one or few angles. The experimental data and the corresponding fits for the Kinney and Perey¹¹ data are shown in Fig. 32.

In addition, data files giving $\bar{\mu}_L$, ξ and γ were generated using the code¹⁴⁰ DUMMY 5 and the data on differential angular distributions. These are given in File 3.

4.2 Inelastic Angular Distribution

The inelastic angular distributions are given as isotropic in the data files. However, analysis of the experimental on the in-elastic angular distributions were done and this will be described briefly below.

In one of the earlier sections^(3,5) it was mentioned that coupled-channel calculations were carried out on the individual nickel isotopes. It is interesting to compare the results of these calculations with data on the differential inelastic scattering to the first excited 2^+ states in these nuclei. As discussed earlier, there are extensive data on the inelastic cross-section of the first excited 2^+ state in ^{58}Ni and ^{60}Ni along with differential angular distributions. The excitation functions of these levels were determined by drawing a smooth curve through the experimental data and joining it to the results of coupled channel calculations at and above 9.0 MeV as it appears reasonable to assume that beyond 9.0 MeV the compound

nuclear contributions to the cross-section are zero and the entire cross-section is due to direct reaction. Below this energy, the compound nuclear and direct reaction cross-sections have to be added to account for both the total magnitude of the inelastic cross-section as well as its angular distribution. Therefore, the direct reaction contribution was subtracted from the evaluated total inelastic cross-section and the differential inelastic distributions from the compound nuclear processes (calculated using CØMMNUC-I) were normalized to this difference. This was then added to the angular distribution given by the coupled channel calculations for comparison with experimental data. It is possible that the total inelastic cross-section given by a particular data set lies above or below the smooth curve. In such a case, the differential angular distributions calculated as above were further normalized to the integral value as given by the experiment. The result of these calculations are shown in Fig. 33-36. In addition, Fig. 37 shows the angular distribution corresponding to inelastic scattering to the first excited states of the nickel isotopes as measured by Clarke and Cross¹⁵, Stelson et. al.⁵⁴ and Kammerdiener²⁶. The curve in this figure corresponds to the calculated direct interaction curve for the isotopes weighted with their natural abundance without any renormalization to the total inelastic scattering cross-section.

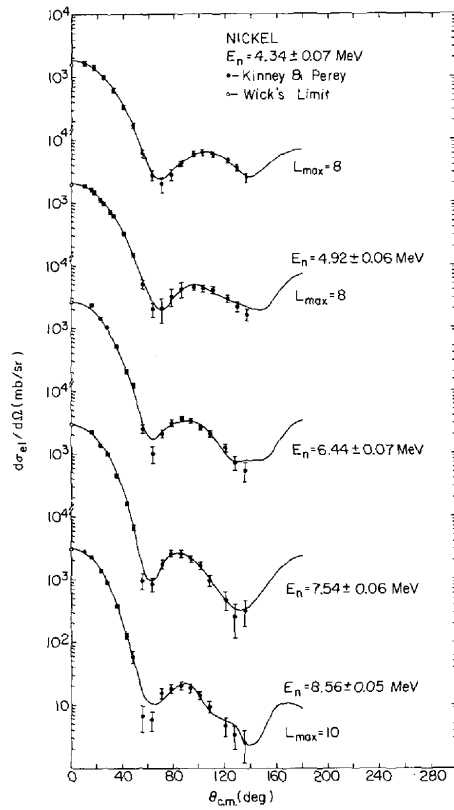
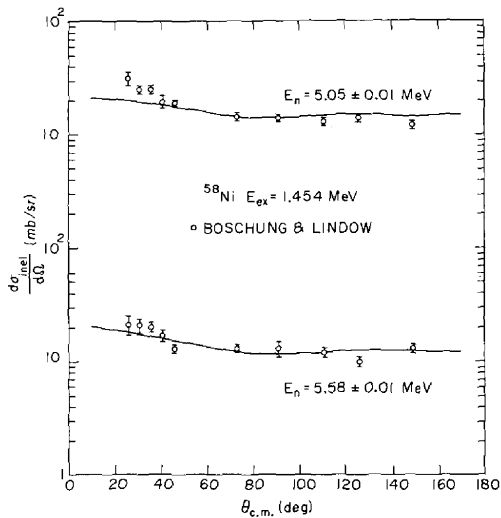


Fig. 32. Differential Elastic Scattering of Ni $E_n = 4.34 - 8.56$ MeV

Fig. 33. Differential Inelastic Scattering of ^{58}Ni $E_{ex} = 1.454$ MeV



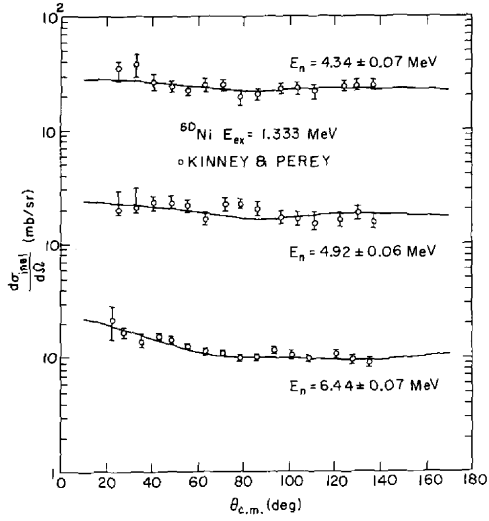


Fig. 34. Differential Inelastic Scattering of ^{60}Ni $E_{\text{ex}} = 1.333$ MeV

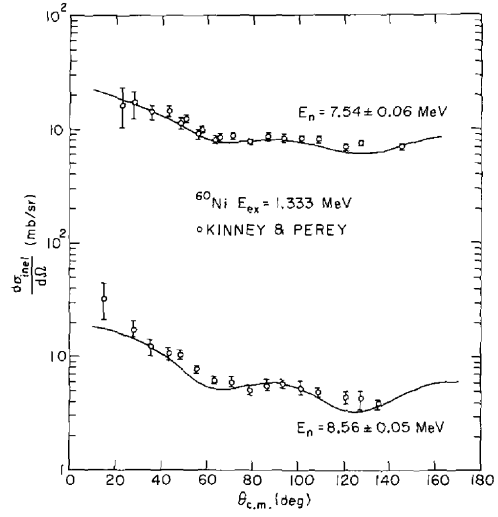


Fig. 35. Differential Inelastic Scattering of ^{60}Ni $E_{\text{ex}} = 1.333$ MeV

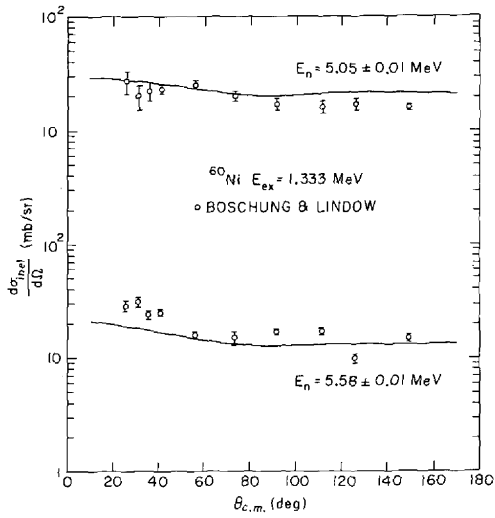


Fig. 36. Differential Inelastic Scattering of ^{60}Ni $E_{\text{ex}} = 1.333$ MeV

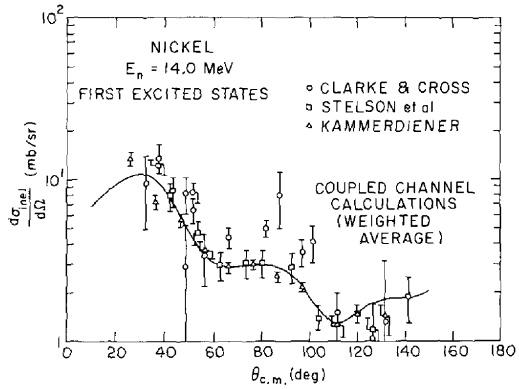


Fig. 37. Differential Inelastic Scattering of Ni $E_n = 14$ MeV

5. The Energy Distribution of Secondary Neutrons

The energy distribution of the secondary neutrons in the (n,2n) and (n,n'p) reactions was determined by using the experimental data of Sal'nikov et. al.³⁸. In this paper, they have a curve showing the energy distribution of neutrons originating from (n,2n) + (n,n'p) processes at an incident energy of 14.4 MeV. The abscissa and ordinates of this curve were read off and it was fitted to an expression of the form $Ae^{-E'/T}$ where E' is the energy of the secondary neutron, and T the temperature. From the least-squares fit the temperature was found to be 0.662 MeV. From the Gilbert and Cameron⁵¹ paper on nuclear level densities, it is found that E_x the energy at which the low excitation energy expression for the level density ($e^{(E-E_0)/T}$) changes over to the high excitation energy expression is 6.3 MeV for ⁵⁹Ni the product of an (n,2n) reaction on ⁶⁰Ni which has a lower Q-value than ⁵⁸Ni. Considering the Q-value of this reaction, this excitation energy is reached at about 14.4 MeV in the laboratory. Hence, it was decided to assign a constant temperature of 0.662 MeV from the threshold of the (n,2n) reaction to 14.4 MeV and from there to 20 MeV calculate the temperature as being proportional to the square root of the excitation energy. Similarly, for the (n,n'p) reaction a constant temperature of 0.662 MeV is given up to 15 MeV and from 15-20 MeV a temperature proportional to the square root of the excitation energy is given.

It has been known for some time¹²⁵⁻¹²⁸ that the energy distribution of the secondary particles in a nuclear reaction cannot be adequately described by a temperature model¹²⁹. This model assumes that secondary particle emission occurs only after the compound nucleus has reached a state of equilibrium and the excitation energy has been distributed amongst all the nucleons. It was pointed out by Griffin¹²⁵ and later elaborated by others¹²⁶⁻¹²⁹ that

there is a finite probability of particle emission before the state of equilibrium is reached and that such emission would give a preponderance of high energy particles. Such a departure of the secondary particle emission from the temperature model has since been verified extensively. It has also been stressed for some time¹³⁰ that ignoring this experimental fact in describing the energy distribution of the secondary particles shows itself in vast differences seen in the results of pulsed sphere experiments as compared to the corresponding calculations. Hence, it was decided to make use of the experimental information on the high-energy component (the pre-equilibrium component) to describe the energy distribution of the inelastically scattered neutrons in the continuum. From Kammerdiener's data²⁶ at 14.6 MeV it is found that the high energy component from 5-12 MeV accounts for about 30% of the total inelastic cross-section. Further, it is assumed that the pre-equilibrium component is zero at 5 MeV incident neutron energy and its energy variation at higher energies is given by a straight-line. With this assumption, the pre-equilibrium component would be estimated from 5 to 20 MeV. In addition, the experimental data of Fujita et. al. and Sal'nikov et. al. obtained a temperature of 1.2 MeV to describe the (n,n') energy distribution at about 14 MeV. From Gilbert and Camerons' paper the transition temperature E_x for ⁵⁸Ni is found to be 10.5 MeV and for ⁶⁰Ni as 9.8 MeV. This is approximately the excitation energy in the final nucleus reached with a laboratory energy of about 10.0 MeV. Therefore, a constant temperature of about 1.0 MeV is given for energies up to 10 MeV and above that the temperature is calculated as being proportional to square root of the excitation energy. With these nuclear temperatures and the preequilibrium fraction determined from Kammerdiener's data, a composite energy distribution was calculated.

Such a distribution is shown in Fig. 38 where the high energy part is shown as a tail appended to the usual distribution given by the temperature model.

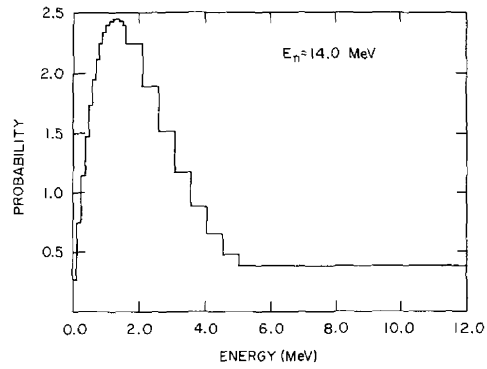


Fig. 38. Energy Distribution of Continuum Scattering $E_n = 14$ MeV

6. Gamma-Ray Production Cross-Section

The data on the gamma-ray production cross-section of nickel can be divided into two distinct parts: the first extends from $1.0E-05$ eV to 1.0 MeV and the gamma rays are assumed to be produced by neutron capture only; the second spans the region from 1-20 MeV and the gamma production cross-section due to all non-elastic processes are given in it. This is possible because the first excited states of the principal even-even isotopes of nickel are above 1.0 MeV and though the (n,p) and (n, α) cross-sections are exoergic these cross-sections are appreciable only above 1.0 MeV.

6.1 Gamma-ray production due to neutron capture

The data on the gamma spectra produced by thermal neutron capture in the natural element are quite extensive. These have been compiled by Bartholomew et. al.¹³¹. However, most of these data sets list only the prominent resolved gamma-ray lines standing above the unresolved continuum. In addition, they might have a rather high cut-off for the γ spectrum. Thus, if the total energy emitted in the thermal capture spectrum of Groshev et. al.¹³² is calculated, it is found to account for only about 70% of the total energy released in capture. Hence, it is important to include the continuum contribution to the γ -ray spectrum and also use data with as low an energy cut-off as possible. Energy resolution of the gamma-ray spectrum is of no consequence for shielding applications as representation of the spectrum in bins 0.5 MeV wide seems to be quite adequate. With these considerations in mind, the data sets used in the present evaluation will be discussed without attempting to describe all the available data.

The thermal neutron capture gamma spectrum in nickel was measured by Maerker and Muckenthaler¹³³ using a calibrated NaI (Tl) detector. The gamma-

ray intensities are given summed up over 0.5 MeV intervals to include both the discrete and continuum gamma rays. The intensities are estimated to have an accuracy of 15%. The low-energy cut-off of their spectrum is at 1.0 MeV; and the total energy released is found to account for 91% of the available energy. The remaining 9% of the energy released is presumably given off by the low energy gamma rays below 1.0 MeV. Hence, to supplement the Maerker and Muckenthaler data, this part of the spectrum was taken from the measurements of Rasmussen et. al.¹³⁴ whose gamma-ray energies go down to 252.3 keV. These data were recorded with a Ge(Li) detector and unfortunately contain a number of spurious peaks either due to impurities in the sample, background gamma-rays or quirks of the peak-fitting program. This is the reason why the total energy released in the spectrum is found to be 10% higher than the maximum possible energy and the data were not used in the evaluation. Since this was the only data set available with such a low energy cut-off; in using these data up to 1.0 MeV, some of the weaker gamma-ray lines were left out and the data were used in this evaluation. These data combined with the Maerker spectrum were renormalized to the Q-value of the capture reaction given in the data files viz: 8.6 MeV. As has been stated earlier, this is an effective binding energy $\bar{B}_n = \frac{\sum B_{ni} a_i \sigma_{nyi}}{\sum a_i \sigma_{nyi}}$ where the summation is over all the isotopes, B_{ni} are their Q-values for capture; a_i their fractional abundances and σ_{nyi} their thermal capture cross-sections as given in Ref. 60. This renormalized data were used to calculate the gamma ray multiplicities from 1.0E - 05 to 4 keV. The resulting of normalized spectral distribution is shown in Fig. 39.

From 4 keV to 100 keV the data of Kenny et. al.¹³⁵ which extends from 4 to 9 MeV gamma-ray energy and were measured from 4 to 80 keV neutron energy were used. In order to fill the gap below 4.0 MeV the capture gamma spectrum given for $E_n = 1.0 \text{ E-05-4 keV}$ was used. The spectra were renormalized to conserve energy and are given at $E_n = 100\text{-}250 \text{ keV}$; $250\text{-}500 \text{ keV}$, $500\text{-}750 \text{ keV}$ and $750 \text{ keV} - 1 \text{ MeV}$. The gamma spectrum corresponding to $E_n = 4 \text{ keV} - 100 \text{ keV}$ is shown in Fig. 40.

6.2 Gamma-ray production cross-section (n,x γ)

Gamma-ray production cross-sections (n,x γ) due to all non-elastic processes given for $E_n = 1\text{-}20 \text{ MeV}$ in the present evaluation are based on the measurements of Dickens et. al.¹³⁶. They measured $\frac{d^2\sigma}{d\omega dE}$ at $\theta_\gamma = 125^\circ$ using a NaI (Tl) spectrometer. The data are presented as gamma-ray production cross-section values of $\frac{d^2\sigma}{d\omega dE_\gamma}$ for $0.7 \leq E_\gamma \leq 10.5 \text{ MeV}$ at various gamma-ray energy intervals and neutron energy bins. Since there are many gamma rays in an E_γ interval one could reasonably assume that their angular distributions are isotropic and multiply the differential cross-sections by 4π to obtain the angle-integrated cross-sections in the corresponding gamma-ray interval. The gamma spectra thus obtained are given in the data files by listing the total production cross-section in MF = 13, MT = 3 and the normalized energy distribution in MF = 15 MT = 3. The energy variation of the total gamma production cross-section is shown in Fig. 41. The data have errors of about 10% from neutron flux measurements, effective area of the beam and absolute efficiency of the detector. In addition, the gamma-production cross-sections have statistical errors of the order of 5% ($E_n = 1.5 - 3.0 \text{ MeV}$) to 27.5% ($E_n = 17 \text{ MeV}$). These have been combined as independent errors to calculate the errors shown in Fig. 41.

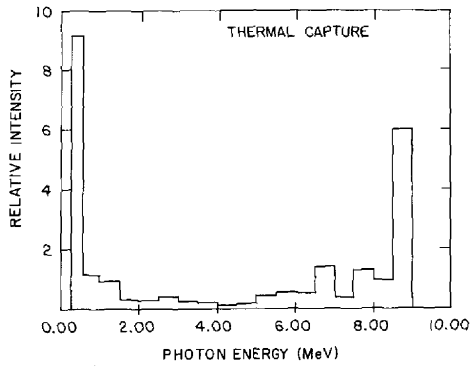


Fig. 39. Normalized Gamma-ray spectrum at Thermal Energies

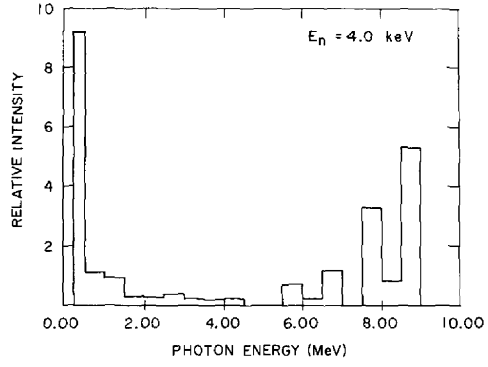


Fig. 40. Normalized Gamma-ray Spectrum $E_n = 4 \text{ keV}$

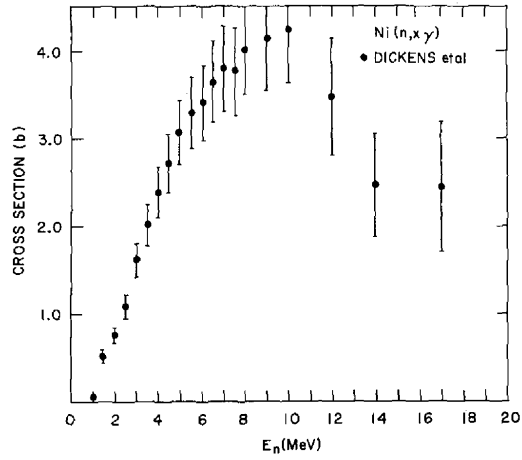


Fig. 41. Gamma-Ray Production Cross-Section $E_n = 1-17 \text{ MeV}$

The above data were used in the evaluation because they are the most extensive and complete data available. There have been some other measurements over limited neutron energy ranges, and it is interesting to compare the Dickens data with these. Perkin¹³⁷ used a three crystal pair spectrometer and measured the gamma production cross-section of nickel over $E_n = 3.5 - 8.5$ MeV at 1.0 MeV intervals. The γ -ray intensities were measured at 90° and the intensities are given summed over 0.5 MeV intervals. The agreement between the two sets of data is satisfactory except in the region $E_\gamma = 1.5 - 2.0$ MeV where the three crystal spectrometer efficiency is low and the background was high. Maerker and Muckenthaler¹³⁸ measured the gamma-spectrum from natural nickel averaged over an incident neutron spectrum from 1 to 14 MeV with a NaI (Tl) detector. Their data are given as $4\pi \frac{d\sigma}{d\Omega} (\Delta E_\gamma, 90^\circ)$ in 0.5 MeV (E_γ) intervals and their overall error is estimated to be 30%. If the Dickens data are averaged over the flux distribution in this experiment and compared with the observed data, the agreement between them is good. In addition, there are measurements by Drake et. al.¹³⁹ of the $\frac{d^2\sigma}{d\Omega dE_\gamma}$ cross-section of nickel at $E_n = 4, 6$ and 7.5 MeV observed at 55° . It is estimated that the errors in these data are about 10%. The agreement between the Drake and the Dickens data is fair. The intensity distribution of the gamma spectra at $E_n = 4, 14$ and 17.0 MeV as given by the Dickens data are shown in Figs. 42-44.

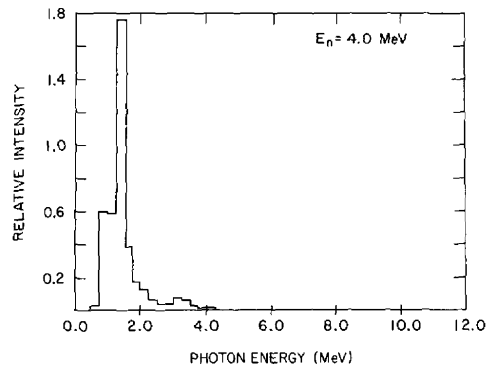


Fig. 42. Ni (n, γ) Spectrum $E_n = 4.0$ MeV

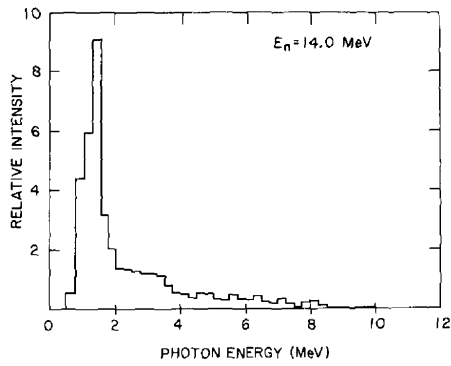


Fig. 43. Ni (n, γ) Spectrum $E_n = 14.0$ MeV

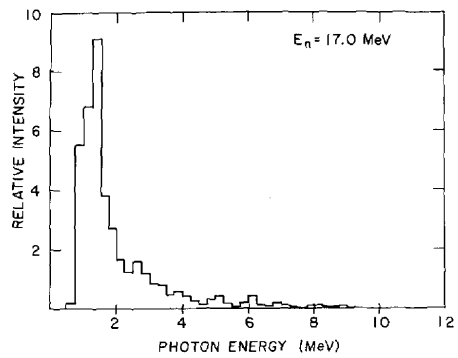


Fig. 44. Ni (n, γ) Spectrum $E_n = 17.0$ MeV

Acknowledgement

This evaluation has greatly benefitted from the experimental data sent by many of my colleagues prior to publication and the discussions I have had with them about their data and its interpretation. This help on their part is greatly appreciated especially as many of them had to find time to organize and send the data in the midst of their other work. It is a great pleasure to express my thanks to: J.D. Anderson, L.F. Hansen and R.J. Howerton of LLL; H.T. Heaton and R.B. Schwartz of NBS; J.K. Dickens, W.E. Kinney and F.G. Perey of ORNL; J.L. Kammerdiener of LASL; M.J. Kenny of AAEC; H. Farrar of AI and E.P. Lippincott of HEDL. I am grateful to Jerry Holm for putting together the gamma-ray files and to the rest of the members of NNCSC who have always been generous with their time and effort whenever their help was needed.

References

1. R.G. Stieglitz, J.T. Reynolds, C.J. Slavik and C.R. Lubitz, Private Communication (1973).
2. N.E. Holden and F.W. Walker, Chart of the Nuclides, 11th Edn, Revised April 1972, Knolls Atomic Power Laboratory and Private Communication (1973).
3. A.H. Wapstra and N.B. Gove, Nuclear Data Tables, 9, 265 (1971).
4. U. Fanger, D. Heck, W. Michaelis, H. Ottmar, H. Schmidt and R. Gaeta Nucl. Phys. A146, 549 (1970).
5. S. Cochavi and W.R. Kane Phys. Rev. 6C, 1650 (1972).
6. S.E. Arnell, R. Hardell, A. Hasselgren, C-G. Mattsson and Ö. Skepstedt. Physica Scripta 4, 89 (1971).
7. Nuclear Level Schemes A=45 through A=257 from Nuclear Data Sheets Edited by Nuclear Data Group ORNL. Academic Press Inc. New York and London 1973.
8. R.B. Schwartz, R.A. Schrack and H.T. Heaton II, NBS Monograph 138 (1973) CSISRS AN - 10416.
9. S. Cierjacks, P. Forti, D. Kopsch, L. Kropp, J. Nebel and H. Unseid KFK-1000 (1968) CSISRS AN-20012.
10. F.G. Perey, T.A. Love and W.E. Kinney, Private Communication (1973) CSISRS AN-10342.
11. W.E. Kinney and F.G. Perey ORNL-4807 (Jan 1974).
12. B. Holmqvist and T. Wiedling AE-366 (1969) CSISRS AN/SN-20019/136-138.
13. A. Langsdorf Jr, R.O. Lane and J.E. Monohan Phys. Rev. 107, 1077 (1957).
14. A.B. Smith, Private Communication CSISRS AN-51595 (1966).
15. R.L. Clarke and W.H. Cross Nucl. Phys. A95, 320 (1967).

16. M.K. Machwe, D.W. Kent Jr and S.C. Snowdon Phys. Rev. 114, 1563 (1959).
17. R.W. Bauer, J.D. Anderson and L.H. Christensen Nucl. Phys. 48, 152 (1963).
18. M. Walt and H.H. Barschall Phys. Rev. 93, 1062 (1954).
19. B. Holmqvist, S.G. Johansson, G. Lodin, M. Salama and T. Wiedling
AE-385 (1970) CSISRS AN/SN-20020/23-27.
20. G.N. Lovchikova Sovt. Jour. At. Energy 13, 648 (1963).
21. I.A. Korzh, N.S. Kopitin, M.V. Pasechnik, N.M. Pravdivii, N.T. Skylar and
I.A. Totskii Journ. Nuc. Energy 19, 141 (1965).
22. L. Ya. Kasakova, V.E. Kolesov, V.I. Popov, O.A. Sal'nikov, V.M. Sluchevskaja,
V.I. Triкова. Int. Conf. on the Study of Nuclear Structure with Neutrons,
Antwerp (1965) p 576.
23. I.A. Korzh, V.A. Mishchenko, M.V. Pasechnik, N.M. Pravdivy, I.E. Sanzhur,
I.A. Totsky YFI-4, 36 (1967).
24. I.A. Korzh, N.S. Kopytin, M.V. Pasechnik, N.M. Pravdivii, N.T. Skylar,
I.A. Totskii, UFZ 8, 1323 (1963).
25. I.A. Korzh, N.T. Skylar UFZ 8, 1389 (1963).
26. J.L. Kammerdiener UCRL-51232 and L.F. Hansen, Private Communication (1973).
27. H.L. Taylor, O. Lönsjö and T.W. Bonner Phys. Rev. 100 174 (1955).
28. V.I. Strizhak, Jour. Nuc. Energy 5, 253 (1957).
29. M.H. MacGregor, W.P. Ball and R. Booth Phys. Rev. 108, 726 (1957).
30. J. R. Beyster, R.L. Henkel, R.A. Nobles and J.M. Kister Phys. Rev. 98,
1216 (1955).
31. J.R. Beyster, W. Walt and E.W. Salmi Phys. Rev. 104, 1319 (1956).
32. M.V. Pasechnik Proc. of the International Conf. on Peaceful Uses of
Atomic Energy Genev 2, 3 (1955).
33. M.K. Machwe, D.W. Kent and S.C. Snowdon, Phys. Rev. 114, 1563 (1959).

34. B. Holmqvist and T. Wiedling, AE-303 (1967).
35. V.I. Kuktevich, B.I. Sinitsin and S.G. Tsipin Jour. Nucl. Energy 11, 46 (1959).
36. A.I. Abrams Sovt. Jour. At. Energy 12, 65 (1962).
37. I. Fujita, M. Sonoda, A. Katase, Y. Wakuta, H. Tawara, M. Hyakutake and K. Iwatani Jour. Nuc. Sci. & Technology 9, 301 (1972).
38. O.A. Sal'nikov, G.N. Lovchikova, G.V. Kotel'nikova, N.I. Fetisov and A.M. Trufanov. Second International Conf. on Nuclear Data for Reactors, Helsinki 2, 359 (1970).
39. D.L. Broder, A.F. Gamalii, A.I. Lashuk and I.P. Sadokhin, Ibid. 2 295 (1970).
40. D.L. Broder, A.I. Lashuk and I.P. Sadokhin ANL-Trans-177 (1964).
41. P. Boschung, J.T. Lindow, E.F. Shrader, Nucl. Phys. A161, 593 (1971).
42. D.L. Broder, V.E. Kolesov, A.I. Lashuk and I.P. Sadokhin, Jour. of Nuc. Energy 18, 645 (1964).
43. R.B. Ray Phys. Rev. 102, 767 (1956), Phys. Rev. 117, 1330 (1960).
44. K. Nishimura, K. Okano and S. Kikuchi, Nucl. Phys. 70, 421 (1965).
45. J.H. Towle and R.O. Owens, Nucl. Phys. A100, 257 (1967).
46. V.C. Rogers, L.E. Beghian and F.M. Clikemann, Nucl. Sci. and Engineering 45, 297 (1971).
47. W.L. Rodgers, E.F. Shrader and J.T. Lindow COO-1573-33, 2. CSISRS AN/SN-50401/11.
48. E.S. Konobeevskii, R.M. Musaelyan, V.I. Popov and I.V. Surkova, Izv. Akad. Nauk SSSR. Ser. Fiz. 35, 2345, 2127 (Tr) (1971).
49. F.G. Perey, C.O. LeRigoleur and W.E. Kinney, ORNL-4523 (1970).
50. C.L. Dunford COMMNUC-I, AI-AEC-12931 (1970).

51. A. Gilbert and A.G.W. Cameron, Can. Journ. Phys. 43, 1446 (1965).
52. C.J. Slavik, KAPL-M-7079 (1971).
53. T. Tamura, ORNL-4152 (1967).
54. P.H. Stelson, R.L. Robinson, J.J. Kim, J. Rapaport and G.R. Satchler, Nucl. Phys. 68, 97 (1965).
55. Nuclear Data Sheets B3 (1970).
56. T. Tamura, Prog. Theor. Phys. Supplement 37/38, 383 (1966).
57. A.B. Smith, P.T. Guenther, P.A. Moldauer and J.F. Whalen, Bull. Amer. Phys. Soc. Ser. II, 19, 111 (1974).
58. B.C. Diven, J. Terrell and A. Hemmendinger, Phys. Rev. 120, 556 (1960).
59. Yu. Ya. Stavisskii and A.V. Shapar, Sovt. Jour. At. Energy 10, 255 (1962).
60. S.F. Mughabghab and D.I. Garber, BNL-325, Vol. 1. 3rd Edn. (1973).
61. J. Benveniste, Proc. of the Second U.N. Int'l Conf. on Peaceful Uses of Atomic Energy 15, 3 (1958).
62. A. Paulsen and H. Liskien Nuk 7, 117 (1965).
63. M. Bormann, F. Dreyer and V. Zielinski EANDC(E) 66, 42 (1966).
64. R.J. Prestwood and B.P. Bayhurst, Phys. Rev. 121, 1438 (1961).
65. J.M.F. Jeronymo, G.S. Marri, J. Olkowsky, A. Sadeghi and G.F. Williamson, Nucl. Phys. 47, 157 (1963).
66. Wen-deh Lu and R.W. Fink, Phys. Rev. C/4, 1173 (1971).
67. W.G. Cross, R.L. Clarke, K. Morin, G. Slinn, N.M. Ahmed and K. Beg, Bull. American Phys. Soc. Ser. II, 7, 335 (1962).
68. J. Csikai EANDC-50, 2 (1965), Conf on Study of Nuclear Structure with Neutrons, Antwerp, paper 102 (1965).
69. M.D. Goldberg, S.F. Mughabghab, B.A. Magurno and V.M. May. BNL-325, Second Ed. Supplement No. 2, Vol. II-A (1966).

70. J.K. Temperley, Nucl. Sci. & Engineering 32, 195 (1968).
71. R.C. Barrall, M. Silbergeld and D.G. Gardner, Nucl. Phys. A138, 387 (1969).
72. R.C. Barrall, M. Silbergeld and D.G. Gardner SUPH-69-2 (1969).
73. R.C. Barrall, J.A. Holmes and M. Silbergeld AFWL-TR-68-134 (1969) CSISRS AN/SN-10022/14.
74. L.A. Rayburn, Phys. Rev. 122, 168 (1961).
75. I.L. Preiss and R.W. Fink, Nucl. Phys. 15, 326 (1960).
76. E.T. Bramlett and R.W. Fink, Phys. Rev. 131, 2649 (1963).
77. R.N. Glover and E. Weigold, Nucl. Phys. 29, 309 (1962).
78. S. Pearlstein, Journ. Nucl. Energy 27, 81 (1973).
79. Z.T. Bódy and C. Csikai, Atomic Energy Reviews 11, 153 (1973).
80. F.L. Hassler and A. Peck Jr. Phys. Rev. 125, 1011 (1962).
81. V.V. Verbinski, T. Hurlimann, W.E. Stephens and E.J. Winhold, Phys. Rev. 108, 779 (1957).
82. L.D. Singletary, E.N. Strait and S.H. Ahn, Phys. Rev. 132, 378 (1963).
83. R.E. Schenter, To be published.
84. H. Liskien and A. Paulsen, Nucl. Phys. 63 393 (1965).
85. H. Liskien and A. Paulsen, Nukleonik, 8, 315 (1966).
86. A. Paulsen, Nukleonik 10, 91 (1967).
87. A. Paulsen, Z. Physik 205, 226 (1967).
88. W.G. Cross, R.L. Clarke, K. Morin, G. Slinn, N.M. Ahmed and K. Beg, Bull. Amer. Phys. Soc. 7, 335 (1962).
89. W.G. Cross, R.L. Clarke, K. Morin, G. Slinn, N.M. Ahmed and K. Beg. EANDC(Can)-16(1963).
90. D.L. Allan, Nucl. Phys. 24, 274 (1961).

91. R.S. Storey, W. Jack and A. Ward, Proc. Phys. Soc. 75, 526 (1960).
92. J.D. Hemingway, Jour. Nucl. Energy 27, 241 (1973).
93. V.N. Levkovskii, G.P. Vinitskaya, G.E. Kovil'skaya and V.M. Stepanov, Sovt. Jour. Nucl. Phys. 10, 25 (1969).
94. P.V. March and W.T. Morton, Phil. Mag. 3, 577 (1958).
95. D.L. Allan, Proc. Phys. Soc. A70, 195 (1957).
96. J.J. VanLoeff, Nucl. Phys. 24, 340 (1961).
97. A.K. Valter, V. Yu. Gonchar, I.I. Zalyubovskii, G.D. Latyshev and G.P. Chursin, Izv. Akad Nauk SSSR. Ser. Fiz. 26, 1079 (1962).
98. U. Seebeck and M. Bormann, Nucl. Phys. 68, 387 (1965).
99. N.A. Khan, S. Mubaraknand and M. Ahmed, Nucl. Phys. A202, 123 (1973).
100. W.G. Slinn and J.M. Robson, Can. Jour. Phys. 41, 545 (1963).
101. C. Spira and J.M. Robson, Nucl. Phys. A127, 81 (1969).
102. V. Levkovskii, G.E. Kovel'skaya, G.P. Vinitskaya, V.M. Stepanov and V.V. Sokd'skii, Sovt. Jour. Nucl. Phys. 8, 4 (1969).
103. Yu-Wen Yu and D.G. Gardner Nucl. Phys. A98, 451 (1967).
104. N.J. Freeman, J.F. Barry and N.L. Campbell, Jour. Nucl. Energy 23, 713 (1969).
105. J. Weitman, N. Daverhög and S. Farvolden, Trans. Amer. Nuc. Soc. 13, 558 (1970).
106. H. Farrar IV, Private Communication (1973).
107. E.P. Lippincott, Private Communication (1974).
108. W.G. Cross and R.L. Clarke, PR-P- 53, 7, 62/ AECL-1542,7,62.
109. I. Kumabe and R.W. Fink, Nucl. Phys. 15, 316 (1960).
110. R.N. Glover and K.H. Purser, Nucl. Phys. 24, 431 (1961).
111. K. Debertin and E. Rössle, Nucl. Phys. 70, 89 (1965).

112. K.R. Alvar, Nucl. Phys. A195, 289 (1972).
113. K.H. Purser and F.W. Titterton, Australian Jour. Phys. 12, 103 (1959).
114. B. Jönsson, K. Nyberg and I. Bergqvist, Arkiv för Fysik 39, 295 (1969).
115. S.A. Cox, Bull. Amer. Phys. Soc. 8, 478 (1963) CSISRS AN-50214.
116. K. Tsukada, S. Tanaka, Y. Tomita and M. Maruyama, Nucl. Phys. A125,
641 (1969).
117. R.W. Hill, Phys. Rev. 109, 2105 (1958).
118. R.L. Becker, W.G. Guindon, G.J. Smith, Nucl. Phys. 89, 154 (1966).
119. V.I. Strizhak, A.O. Kozar and M.S. Nazarov, Ukrainian Jour. of Phys.
5, 704 (1960).
120. M.J. Poole, Phil. Mag. 44, 1398 (1954).
121. J.B. Weddell, Phys. Rev. 104, 1069 (1956).
122. S. Berko, W.D. Whitehead and B.C. Groseclose, Nucl. Phys. 6, 210 (1958).
123. E.H. Auerbach, ABACUS-2, BNL 6562 (1964).
124. R.F. Berland CHAD, NAA-SR-11231 (1965).
125. J.J. Griffin, Phys. Rev. Letters 17, 478 (1966).
126. M. Blann, Phys. Rev. Letters 21, 1357 (1968).
127. F.C. Williams, Phys. Letters 31B, 184 (1970).
128. J.M. Miller, Proc. of the International Conf. on Nuclear Physics,
Munich, 2, 597 (1973).
129. J.M. Blatt and V.F. Weisskopf, Theoretical Nuclear Physics, John Wiley &
Sons, New York (1952).
130. L.F. Hansen, J.D. Anderson, P.S. Brown, R.J. Howerton, J.L. Kammerdiener,
C.M. Logan, E.F. Plachaty and C. Wong, Nucl. Sci. and Engineering 51,
278 (1973).

131. G.A. Bartholomew, A. Doveika, K.M. Eastwood, S. Monaro, L.V. Groshev, A.M. Demidov, V.I. Pelekhov and L.L. Sokolovskii, Nuclear Data 3A, 367 (1967).
132. L.V. Groshev, A.M. Demidov, N. Shadiev, Sov. Jour. Nucl. Phys. 3, 319 (1966).
133. R.E. Maerker and F.J. Muckenthaler, ORNL-4382 (1969).
134. N.C. Rasmussen, V.J. Orphan, T.L. Harper, J. Cunningham and S.A. Ali, DASA 2570 (GA-10248) (1970).
135. M.J. Kenny, P.W. Martin and J.R. Bird. Private Communication (1973).
136. J.K. Dickens, T.A. Love and G.L. Morgan ORNL-TM-4379 (1973).
137. J.L. Perkin, Nucl. Phys. 60, 561 (1964).
138. R.E. Maerker and F.H. Muckenthaler, Nucl. Sci. Eng. 42, 335 (1970).
139. D.M. Drake, J.C. Hopkins, C.S. Young and H. Condé, Nucl. Sci. and Eng. 40, 294 (1970).

Table 1
Properties of the Naturally Occurring Nickel Isotopes

Isotope	Fractional Abundance	Isotopic Mass
^{58}Ni	0.683	57.9353358
^{60}Ni	0.261	59.9307795
^{61}Ni	0.011	60.9310502
^{62}Ni	0.036	61.9283396
^{64}Ni	0.009	63.927956

Table 2
Reaction Q-Values for the Nickel Isotopes

Reaction	Q-Value (MeV)				
	^{58}Ni	^{60}Ni	^{61}Ni	^{62}Ni	^{64}Ni
(n, γ)	8.9993	7.8195	10.5962	6.8376	6.0976
(n, p)	0.3947	-2.0411	-0.5252	-4.4343	-6.2168
(n, d)	-5.9526	-7.3081	-7.6360	-8.8964	-10.3114
(n, t)	-11.0724	-11.5107	-8.8700	-11.9750	-12.4600
(n, ^3He)	-6.4856	-9.1841	-10.4171	-12.1776	--
(n, α)	2.8902	1.3514	3.5749	-0.4352	-2.4315
(n, np)	-8.1772	-9.5327	-9.8606	-11.121	-12.536
(n, n α)	-6.4083	-6.2948	-6.4681	-7.0217	-8.100
(n, 2n)	-12.203	-11.3883	-7.8195	-10.5966	-9.6596

Table 3
The Elastic Scattering Cross-Section for Nickel

E_n (MeV)	σ_{el} (b)	Reference
0.06	10.0±1.0	A. Langsdorf Jr. et. al. Ref. 13. $\Delta E_n=100-60\text{keV}$.
0.135	7.34±.73	"
0.228	5.66±.57	"
0.312	4.79±.48	"
0.396	4.18±.42	"
0.477	4.18±.42	"
0.558	3.40±.34	"
0.640	3.97±.40	"
0.723	3.15±.32	"
0.804	3.09±.31	"
0.882	3.13±.31	"
0.970	3.01±.3	"
1.044	2.59±.26	"
1.128	2.80±.28	"
0.7	3.84	A.B. Smith Ref. 14. $\Delta E_n=20\text{keV}$. Only a few of the 91 data points are listed.
0.706	3.89	"
0.725	3.4	"
0.750	3.06	"
0.8	3.42	"
0.849	3.49	"
0.899	3.69	"
0.972	3.3	A.B. Smith Ref. 14. $\Delta E_n=20\text{keV}$. Only a few of the 91 data points are listed.
1.035	3.27	"
1.11	3.03	"
1.204	3.02	"
1.299	3.41	"
1.399	3.26	"
1.456	3.36	"
14.1±0.9	1.2±1.2	R.L. Clarke and W.G. Cross Ref. 15.

Table 3 (contd)
The Elastic Scattering Cross-Section for Nickel

E_n (MeV)	σ_{el} (b)	Reference
3.66±0.4	1.82±0.1	M.K. Machwe et. al. Ref. 16.
14.0	1.23±0.1	R.W. Bauer et. al. Ref. 17.
1.0	2.8	M. Walt and H.H. Barschall Ref. 18.
3.0±0.05	2.15±.11	B. Holmqvist and T. Wiedling Ref. 12.
3.49±.05	2.06±.10	"
4.0±.05	2.0±.10	"
4.56±.05	2.0±.10	"
6.09±.09	1.83±.09	"
7.05±.09	1.79±.09	"
8.05±.09	1.71±.09	"
1.77±.05	1.88±.19	B. Holmqvist et. al. Ref. 19.
2.02±.05	2.13±.21	"
2.27±.05	1.85±.19	B. Holmqvist et. al. Ref. 19.
2.52±.05	2.49±.25	"
2.76±.05	2.36±.25	"
0.9	3.2±0.24	G. N. Lovchikova Ref. 20.
0.5±.05	3.57±.012	I. A. Korzh et. al. Ref. 21.
0.8±.05	3.15±.15	"
2.0±.1	2.5	L. Ya Kasakova et. al. Ref. 22.
1.5	2.765±.105	I. A. Korzh et. al. Ref. 23.
0.65±.05	3.57±.12	I. A. Korzh et. al. Ref. 24.
0.3±.025	4.68±.18	I. A. Korzh et. al. Ref. 25.
4.34±.07	2.077±.150	W. E. Kinney and F. G. Perey Ref. 11.
4.92±.06	1.898±.137	"
6.44±.07	2.101±.153	"
7.54±.06	1.935±.143	"
8.56±.05	1.887±.138	"
14.6	1.174±.117	Kammerdiener Ref. 26.

Table 4

The Non-Elastic Scattering Cross-Section Data for Nickel

E_n (MeV)	$\sigma_{\text{non-el}}$ (b)	Reference
14.0	1.44±.12	R.W. Bauer et. al. Ref. 17.
3.5	1.48±.04	H.L. Taylor et. al. Ref. 27.
4.7	1.54±.06	"
7.1	1.33±.06	"
12.7	1.35±.05	"
14.1	1.45±.05	"
14.0	1.38±.05	V.I. Strizhak. Ref. 28.
14.2±.3	1.38±.03	M.H. MacGregor et. al. Ref. 29.
1.0	0.1	M. Walt and H.H. Barschall Ref. 18.
4.0±.07	1.35±.1	J.R. Beyster et. al. Ref. 30.
4.5±.07	1.50±.06	
1.0±.08	0.06±.03	J.R. Beyster et. al. Ref. 31.
2.5±.08	0.8±.06	"
7.0±0.4	1.48±.06	"
2.5	0.83±.12	M.V. Pasechnik. Ref. 32.
3.3	1.35±.25	"
3.66±.4	1.51±.18	M.K. Machwe et. al. Ref. 33.
3.03±.05	1.12±.14	B. Holmqvist and T. Wiedling. Ref. 34.
3.49±.05	1.43±.12	"
4.0±.05	1.51±.12	"
4.56±.05	1.63±.12	"
6.09±.10	1.91±.13	B. Holmqvist and T. Wiedling. Ref. 34.
7.05±.10	1.78±.13	"
8.05±.10	1.82±.13	"
2.9±.10	1.9±.03	V.I. Kuktevich, et. al. Ref. 35.
1.5	0.05±.05	A.I. Abramov. Ref. 36.
1.6	0.21±.1	"
1.8	0.46±.12	"
2.0	0.6±.1	"
2.2	0.75±.1	"
2.4	0.85±.1	"

Table 5
The Total Inelastic Scattering Cross-Section for Nickel

E_n (MeV)	$\sigma_{(nn')\text{Total}}^{(b)}$	Reference
14.0	0.766±.078	I. Fujita et. al. Ref. 37.
14.4±.14	0.76±.04	O.A. Sal'nikov et. al. Ref. 38.
3.79	1.20	D.L. Broder et. al. Ref. 39.
4.01	1.24	"
4.39	1.23	"
4.5	1.25	"
4.84	1.21	"
5.17	1.19	"
5.42	1.03	"
1.4	0.16	D.L. Broder et. al. Ref. 40.
1.5	0.35	"
1.6	0.45	"
1.8	0.56	"
2.0	0.62	"
2.2	0.66	"
2.4	0.70	"
2.5	0.78	"
3.5	1.19	"
4.0	1.31	"

Table 6
The Optical Model Parameters

Radial shape of real well	Saxon-Woods
Real well depth - Ni	49.61333
Real well depth - Ni ⁵⁸	49.95644
Real well depth - Ni ⁶⁰	49.06173
Real well depth - Ni ⁶¹	48.63638
Real well depth - Ni ⁶²	48.22474
Real well depth - Ni ⁶⁴	47.44007
Real well radius	1.25 A ^{1/3}
Real well diffuseness	0.68893
Radial shape of imaginary well	Saxon-Woods derivative
Imaginary well depth	11.46508
Imaginary well radius	1.25 A ^{1/3}
Imaginary well diffuseness	0.41562
Radial shape of spin-orbit well	Saxon-Woods derivative
Spin-orbit well depth	7.10
Spin-orbit well radius	1.25 A ^{1/3}
Spin-orbit well diffuseness	0.68893
Energy dependence of real well depth	-0.333,E

Table 7

Summary of Data on $(n,n'p)$, (n,pn') and or (n,d) Cross-Section for Nickel

Target	E_n (MeV)	Method	Cross-Section	σ (mb)	Reference
^{58}Ni	14.5	Activation	$\sigma(n,n'p)+\sigma(n,d)$	680±80	W.G. Cross et. al. Ref. 67.
^{58}Ni	13.58	"	"	513	W.G. Cross & R.L. Clarke Ref. 108.
^{58}Ni	14.07	"	"	615	"
^{58}Ni	14.73	"	"	685	"
^{58}Ni	14	Phot Emulsion	$\sigma(n,n'p)$	343±27	D.L. Allan Ref. 90.
^{60}Ni	14	"	"	51±9	"
^{58}Ni	14.8	"	$\sigma(n,n'p)$	150	I. Kumake & R.W. Fink Ref. 109.
^{58}Ni	14.7	Activation	$\sigma(n,n'p)+\sigma(n,d)$	520±120	Bramlett & Fink, Ref. 76.
^{58}Ni	14.8±.2	"	"	750±60	Barrall et. al., Ref. 71.
^{58}Ni	14.5±.2	"	"	750±70	Barrall et. al., Ref. 72.
^{58}Ni	13.72±.2	"	$\sigma(n,n'p)+\sigma(n,pn')+\sigma(n,d)$	595±71	F.K. Temperley Ref. 70.
^{58}Ni	13.95±.2	"	"	642±77	"
^{58}Ni	14.20±.25	"	"	544±65	"
^{58}Ni	14.31±.30	"	"	527±63	"
^{58}Ni	14.53±.32	"	"	516±62	"
^{58}Ni	14.79±.3	"	"	497±60	"
^{58}Ni	14.6±.2	"	$\sigma(n,n'p)+\sigma(n,d)$	730±60	Barrall et. al. Ref. 73.
^{58}Ni	14	Phot Emulsion	$\sigma(n,n'p)$	220±44	D.L. Allan Ref. 95.
^{58}Ni	14.8	Counter Telescope	$\sigma(n,n'p)$	340±34	Glover & Purser Ref. 110.
^{58}Ni	14.1	Activation	$\sigma(n,n'p)+\sigma(n,pn')+\sigma(n,d)$	540±50	Glover & Weigold Ref. 77.
^{58}Ni	14.8	Activation	$\sigma(n,n'p)+\sigma(n,pn')+\sigma(n,d)$	570±55	Glover & Weigold Ref. 77.
^{58}Ni	14.7	Activation	$\sigma(n,n'p)+\sigma(n,pn')+\sigma(n,d)$	619±49	Hemingway Ref. 92.
^{58}Ni	8.4	Counter Telescope	$\sigma(n,d)$	23.5±4	Debertin & Rössle Ref. 111.
^{58}Ni	14.4	Activation	$\sigma(n,n'p)+\sigma(npn')+\sigma(n,d)$	509±51	Lu & Fink Ref. 66.
^{58}Ni	14.1	Counter Telescope	$\sigma(n,n'p)$	224±16	Alvar Ref. 112.
^{60}Ni	13.5±.1	Phot Emulsion	$\sigma(n,n'p)$	68	March & Morton Ref. 94.
^{62}Ni	14.5	Activation	$\sigma(n,n'p)$	4.4±1.0	Cross et. al. Ref. 89.
^{62}Ni	14.8±.9	"	$\sigma(n,n'p)$.65±.15	Preiss & Fink Ref. 75.
^{62}Ni	14.1	"	$\sigma(n,n'p)$	4	Valter et. al. Ref. 97.
^{64}Ni	14.8±.9	"	$\sigma(n,n'p)$.93±.04	Preiss & Fink Ref. 75.
^{64}Ni	14.1	"	$\sigma(n,n'p)$	6	Valter et. al. Ref. 97.

Table 8
 Error Estimates of the Evaluated Cross Sections of Ni
 ENDF/B-IV MAT No. 1190

Cross Section	.ENDF/B Designation		Neutron Energy (MeV)									
	MF	MT	Resonance		1	2	3	5	10	15	20	
			Thermal	10-11-0.69								
Total	3	1	5%	5-10%	1.5%	1.5%	2%	2%	2%	3%	3%	
Elastic	3	2	3%	16-27%	20%	16%	13%	6%	7%	8%	8%	
Total (n,n')	3	4	-	-	-	40%	40%	40%	30%	30%	30%	
Discrete (n,n')	3	51	-	-	-	30%	30%	30%	10%	10%	10%	
	3	52	-	-	-	12%	10%	10%	10%	10%	10%	
	3	53	-	-	-	14%	15%	16%	10%	10%	10%	
Other Discrete (n,n')	3	54-65	-	-	-	40%	40%	40%	30%	30%	30%	
Continuum (n,n')	3	91	-	-	-	40%	40%	40%	30%	30%	30%	
(n,2n)	3	16	-	-	-	-	-	-	15%	15%	15%	
(n,n'p)	3	28	-	-	-	-	-	-	200%	200%	200%	
(n, γ)	3	102	4%	15-25%	20%	20%	20%	20%	20%	20%	20%	
(n,p)	3	103	-	-	10%	10%	5%	5%	5%	5%	10%	
(n, α)	3	107	-	-	-	-	20%	20%	20%	20%	20%	
Gamma Prod. (n, γ)	12	102	15%	20%	20%	-	-	-	-	-	-	
(n,x γ)	13	3	-	-	-	11%	11%	12%	15%	23%	29%	

